

Density Functional Theory Studies of MoS₂

A Dissertation for
PHY-651 - Dissertation
Credits: 16

Submitted in partial fulfillment of Masters Degree

M.Sc in Physics (Computational Physics)

Goa University

in the subject of Physics

by

Shantanu Bhanudas Naik

Seat number: 22P0430037

ABC Id: 679711891301

PRN: 201905605

Under the supervision of

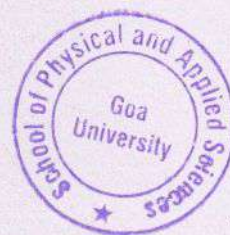
Dr. Bhargav K. Alavani

School Of Physical and Applied Science
Physics discipline



Goa University

May 2024



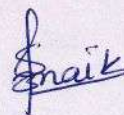
Examined by:

A handwritten signature in blue ink, appearing to be 'R. V.' with a long horizontal stroke.

Seal of the School

DECLARATION

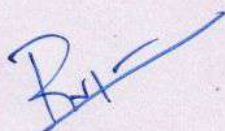
I hereby declare that the work presented in this dissertation, titled "Density Functional Theory studies of MoS₂", is based on my original research conducted under the supervision of Dr. Bhargav Alavani, at Goa University. This work has not been previously submitted for any degree or diploma at this university or any other institution. To the best of my knowledge, it does not contain any material previously published or written by another person except where due acknowledgment has been made in the text.



Shantanu B. Naik

COMPLETION CERTIFICATE

This is to certify that the dissertation report "Density Functional Theory Studies of Molybdenum Di-Sulphide" is a bonafide work carried out by Shantanu Naik under the supervision of Dr. Bhargav Alavani in partial fulfillment of the requirements for the award of the degree of the Master of Science in Physics at the School of Physical and Applied Science, Goa University.



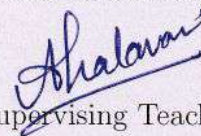
Signature of the Dean of the School

Date: 09/05/2024

Place: Goa University



Seal of the School



Signature of Supervising Teacher

Dr. Bhargav Alavani

PREFACE

The dissertation titled "Density Functional Theory Studies of MoS₂" was conducted under the guidance of Dr. Bhargav Alavani. The project aimed to study the structural and electronic properties of monolayer, bilayer, and bulk MoS₂. Additionally, the study examined the dependence of the band structure on interlayer distance.

ACKNOWLEDGEMENT

"I would like to express my sincere gratitude to Dr. Bhargav Alavani, my project guide, for his invaluable guidance and unwavering support in helping me complete my project titled "Density Functional Theory Studies of Molybdenum Di-Sulphide". I would also like to thank the faculty of the School of Physical and Applied Sciences (SPAS) for providing me with the necessary resources to complete my project. Lastly, I am grateful to God for the successful completion of my project."

ABSTRACT

Molybdenum disulphide has garnered significant attention due to its unique properties and potential applications in various fields such as electronics, energy storage, and catalysis. Density functional theory calculations have become an useful tool for studying the properties of materials. In this project, we aim to perform density functional theory calculations to investigate molybdenum disulphide's structural and electronic properties. We studied the evolution of its electronic properties from monolayer, bilayer, and bulk by studying the band structure. Also, a detailed study of the dependence of interlayer distance on the nature of the band structure was carried out.

List of Figures

2.1	Plot shows all electron valence wavefunctions (left) and pseudized valence wavefunction (right)	12
2.2	Self Consistent field (SCF) Loop for the	14
3.1	This figure shows a visualization of MoS ₂ monolayer from top and side. . .	19
3.2	Above figure shows plot of SCF energy w.r.t kinetic energy cut off both in units of Ry.	20
3.3	Above figure shows the plot of SCF energy w.r.t discretized k vector (or k-points) grid.	21
3.4	Above figure shows plot of SCF energy w.r.t lattice constant in Ang done with GGA exchange-correlation using PAW pseudopotential	21
3.5	Above figure shows plot of electron dispersion curve and TDOS of MoS ₂ .	22
3.6	Above figure shows the plot of TDOS and PDOS (Left) PDOS of sulfur (Right) PDOS of Molybdenum	23
3.7	Above figure shows the plot of spin-orbit coupling in monolayer MoS ₂ , (a) Without spin-orbit coupling (b) with spin-orbit coupling.	24
3.8	Above figure shows plot of SCF energy w.r.t kinetic energy cut off both in units of Ry.	25
3.9	Above figure shows the plot of SCF energy w.r.t discretized k vector (or k-points) grid.	26
3.10	Above figure shows plot of electron dispersion curves of MoS ₂ , a) Band structure obtained using vdw-df-C6 b) Band structure obtained using vdw-df3-opt1 c) Band structure obtained using vdw-df3-opt2 d) Band structure obtained using Grimme-df2 e) Band structure obtained using LDA f) Band structure obtained using GGA.	28

3.11	Above figure shows plot of TDOS and PDOS (Left) PDOS of sulfur (Right) PDOS of Molybdenum	31
3.12	Above figure shows plot of SCF energy w.r.t kinetic energy cut off both in units of Ry.	32
3.13	Above figure shows the plot of SCF energy w.r.t discretized k vector (or k points) grid.	33
3.14	Above figure shows plot of electron dispersion curves of MoS ₂ , a) Band structure obtained using vdw-df-C6 b) Band structure obtained using vdw-df3-opt1 c) Band structure obtained using vdw-df3-opt2 d) Band structure obtained using Grimme-df2 e) Band structure obtained using LDA f) Band structure obtained using GGA.	35
3.15	Above figure shows plot of TDOS and PDOS (Left) PDOS of sulfur (Right) PDOS of Molybdenum	37
3.16	Comparison of the Band structure of a) monolayer, b) bilayer and c) bulk MoS ₂	38
3.17	This figure compares of density of states of monolayer bilayer and bulk MoS ₂	39
3.18	This figure compares the nature of planar charge density and planar potential energy for bilayer MoS ₂ , subplot 3.18a is for reference and shows how Sulfur (yellow region) and Molybdenum (red region) contribute to planar charge density.	40

Contents

1	Introduction	1
1.1	Literature Review	1
1.2	Motivation	2
1.3	Objectives	2
2	Method	3
2.1	Formalism	3
2.1.1	Many Body Hamiltonian	3
2.2	Hohenberg-Kohn Theorems	5
2.2.1	1 st Hohenberg-Kohn Theorem	5
2.2.2	2 nd Hohenberg-Kohn Theorem	7
2.3	Kohn-Sham Equations	7
2.4	Approximations	9
2.4.1	Exchange-Correlation Functional	9
2.4.2	Pseudopotentials	11
2.5	Plane wave method	13
2.6	Self Consistent Field method	13
2.7	Structural Optimization	15
2.8	Band Structure	16
2.9	Density of states	16
2.10	vdW functionals	17
3	Results	19
3.1	Brief	19
3.2	Monolayer	19

3.2.1	Convergence tests	20
3.2.2	Volume Optimization	21
3.2.3	Electronic Properties	22
3.2.4	Spin Orbit Coupling	23
3.3	Bilayer	25
3.3.1	Convergence tests	25
3.3.2	Volume Optimization	26
3.3.3	Electronic Properties	28
3.4	Bulk	32
3.4.1	Convergence tests	32
3.4.2	Volume Optimization	33
3.4.3	Electronic Properties	35
	References	41

Chapter 1

Introduction

In recent years, there has been a lot of research on 2D layered materials due to their unique properties and reduced dimensionality. These materials have opened doors for various applications in electronics, medicine, and other fields of interest. One such material that has attracted a lot of attention is Transition Metal Dichalcogenides (TMDs). TMDs are materials where transition metal atoms bond with chalcogen atoms (such as Sulfur, Selenium, or Tellurium) in a layered structure. TMDs have unique electronic, optical, and mechanical properties which make them suitable for applications in optoelectronics, electronics, catalysis, energy storage, and sensing.

Molybdenum Disulphide (MoS_2) is a popular TMD because of its peculiar electronic properties, making it a good candidate for a research topic. This dissertation uses the Density functional theory to conduct a detailed study of MoS_2 . This project studies the electronic and other properties of monolayer, bilayer, and bulk MoS_2 .

1.1 Literature Review

Molybdenum disulfide (MoS_2) is a material that has optoelectric and electronic applications due to its layered structure. Due to its large band gap, Monolayer MoS_2 is particularly useful in semiconductor applications. This project focuses on a detailed study of monolayer, bilayer, and bulk MoS_2 . The experimental work in these different structures of MoS_2 suggests the transition of indirect band gap seen in bulk MoS_2 into direct one in monolayer MoS_2 [1].

The choice of exchange-correlation functional affects the band structure [2]. It is seen

that GGA gives the correct band gap but its band structure nature is not accurate. A correction of Grimme df2 [3] gives the correct nature of the band but underestimates [2].

1.2 Motivation

MoS₂, in particular, stands out as a promising candidate for various applications in electronics, optoelectronics, catalysis, energy storage, and sensing due to its exceptional electronic properties. However, a comprehensive understanding of how these properties vary depending on the number of layers (monolayer, bilayer, or bulk) is crucial for optimizing MoS₂ for specific applications.

This project aims to bridge this knowledge gap by employing Density Functional Theory (DFT) to conduct a meticulous investigation of MoS₂. By studying the electronic and other properties of the monolayer, bilayer, and bulk MoS₂, this research will provide valuable insights into the impact of dimensionality on MoS₂'s behavior.

1.3 Objectives

In this project, we employ density functional theory (DFT) to calculate different structural and electronic properties of the MoS₂. The main objectives of the project are as follows

1. To study structure properties such lattice constants and interlayer distances in monolayer bilayer and bulk MoS₂.
2. To study electronic properties such band structure and density of states interlayer in monolayer bilayer and bulk MoS₂.

Chapter 2

Method

Density Functional Theory (DFT) is a framework based on quantum mechanics that allows scientists to study the properties of materials from scratch, without needing any prior assumptions. DFT is different from the Hartree-Fock (HF) method but shares its approach to studying material properties. DFT also introduces simplifications and modifications that make it more effective at studying the electronic structure of many-body systems. In this chapter, we will discuss the key elements of DFT, including its core formalism, and the techniques used to enhance its computational efficiency and accuracy. core formalism, and the techniques used to enhance its computational efficiency and accuracy.

2.1 Formalism

2.1.1 Many Body Hamiltonian

From the first principle considerations, we can write a many-body Hamiltonian for a solid or the simplest case i.e. a molecule. The said Hamiltonian is given below

$$\hat{H} = -\sum_{i=1}^N \frac{\nabla_i^2}{2} - \sum_{A=1}^N \frac{\nabla_A^2}{2} + \sum_{A=1}^N \sum_{B=1}^N \frac{1}{|R_A - R_B|} - \sum_{A=1}^N \sum_{i=1}^N \frac{1}{|r_i - R_A|} + \sum_{i=1}^N \sum_{j=1}^N \frac{1}{|r_i - r_j|} \quad (2.1)$$

To get a good understanding of the above Hamiltonian we can write it as

$$\hat{H} = \hat{T}_{ion}(\vec{R}) + \hat{T}_{elec}(\vec{r}) + \hat{V}_{ion-ion}(\vec{R}) + \hat{V}_{ion-elec}(\vec{R}, \vec{r}) + \hat{V}_{elec-elec}(\vec{r}) \quad (2.2)$$

The terms $\hat{T}_{ion}(\vec{R})$ and $\hat{T}_{elec}(\vec{r})$ are terms corresponding to the kinetic energy of positive ions and electrons respectively. Whereas $\hat{V}_{ion-ion}(\vec{R})$, $\hat{V}_{ion-elec}(\vec{R}, \vec{r})$ and $\hat{V}_{elec-elec}(\vec{r})$ are terms that correspond to ion-ion, ion-electron, and electron-electron potential.

The above Hamiltonian depends on both nuclear and electronic contributions. To get a Hamiltonian that only depends on electronic contributions, we can make use of some approximations.

The need to use approximations for the above Hamiltonian is crucial as we have to keep track of nuclear as well as electronic parameters. A better approximation would be to focus on only one type of contribution to Hamiltonian in this case it would be the electronic contribution that we are interested in. The approximation that helps to achieve this is **Born Oppenheimer approximations**.

The Born Oppenheimer approximation is an approximation that allows us to separate the above Hamiltonian into nuclear and electronic contributions. In these approximations, we consider that since ions are 1800 times more massive than electrons, the electrons will respond to external perturbation more quickly than ions. Thus we can consider ions to be fixed and thus modify our Hamiltonian accordingly.

The equation 2.2 becomes

$$\hat{H} = \hat{T}_{elec}(\vec{r}) + \hat{V}_{ion-ion}(R) + \hat{V}_{ion-elec}(R, \vec{r}) + \hat{V}_{elec-elec}(\vec{r}) \quad (2.3)$$

The Born Oppenheimer approximation does the following changes to the above Hamiltonian:

1. The kinetic term related to ions is neglected as ions are considered to be fixed.
2. Since ions are fixed, R is constant. Therefore the dependence on R is considered constant or parametric. Therefore term $\hat{V}_{ion-ion}(R)$ is constant and term $\hat{V}_{ion-elec}(R, \vec{r})$ is parametric.

The constant term i.e. $\hat{V}_{ion-ion}(R)$ will add some constant value to the expectation value of other operators hence we can keep that constant value as a reference, therefore, equation 2.3 now our Hamiltonian will have the following form

$$\hat{H}_{elec} = \hat{T}_{elec}(\vec{r}) + \hat{V}_{ion-elec}(R, \vec{r}) + \hat{V}_{elec-elec}(\vec{r}) \quad (2.4)$$

Hence now our Hamiltonian has electronic contributions only. Hence we can now write a many-body Schrodinger equation.

$$\hat{H}_{elec}\Psi(r) = E(R)\Psi(r) \quad (2.5)$$

Nuclear coordinates now parameterize the equation. This above equation is the central or beginning step to doing many of the electronic structure methods.

2.2 Hohenberg-Kohn Theorems

Now although we have an electronic Hamiltonian to work with solving it is a tedious task in itself. We have to solve the equation 2.5 to get a wave function that describes the system's ground state. The use of variational techniques and proper constraints can give us a proper solution, which is a standard approach in Hartree and Hartree Fock method. In DFT, however, we are going beyond this and trying to define the system's ground state not with some ground state wavefunction but with density using two fundamental theorems that are the backbone of DFT. Hohenberg and Kohn in their paper [4] gave us these two fundamental theorems.

2.2.1 1st Hohenberg-Kohn Theorem

The 1st Hohenberg-Kohn theorem states that the ground state of any interacting many body/particle system is a unique functional of electron density $n(\vec{r})$. The proof of this rather simpler one goes as follows;

Let us consider two different external potentials (ion-electron potentials) given by $\hat{V}_{ion-elect}(\vec{r})$ and $\hat{V}'_{ion-elect}(\vec{r})$ gives us same electron density $n(\vec{r})$. The corresponding Hamiltonian will be \hat{H} and \hat{H}' and all other terms will represent with \hat{G} which are the same if we consider the same system for both potentials having some N number of atoms. Hence we can write

$$\hat{H} = \hat{G} + \hat{V}_{ion-elect}(\vec{r}) \quad \text{and} \quad \hat{H}' = \hat{G} + \hat{V}'_{ion-elect}(\vec{r}) \quad (2.6)$$

The total energy of the system is given by

$$E = \langle \psi | \hat{H} | \psi \rangle \quad \text{and} \quad E' = \langle \psi' | \hat{H}' | \psi' \rangle \quad (2.7)$$

where ψ and ψ' are the ground state wavefunctions of the system. Here $E \neq E'$ because the potentials are not the same. According to the variational principle, we have:

$$\begin{aligned} E' &< \langle \psi | \hat{H}' | \psi \rangle = \langle \psi | \hat{H}' - \hat{V}'_{ion-elec}(\vec{r}) + \hat{V}_{ion-elec}(\vec{r}) | \psi \rangle \\ &= E + \langle \psi | \hat{V}'_{ion-elec}(\vec{r}) - \hat{V}_{ion-elec}(\vec{r}) | \psi \rangle \end{aligned} \quad (2.8)$$

and

$$\begin{aligned} E &< \langle \psi' | \hat{H} | \psi' \rangle = \langle \psi' | \hat{H} - \hat{V}_{ion-elec}(\vec{r}) + \hat{V}'_{ion-elec}(\vec{r}) | \psi' \rangle \\ &= E' + \langle \psi' | \hat{V}_{ion-elec}(\vec{r}) - \hat{V}'_{ion-elec}(\vec{r}) | \psi' \rangle \end{aligned} \quad (2.9)$$

By adding Eqs. 2.8 and 2.9, we obtain:

$$(E + E') < (E + E') + \langle \psi | \hat{V}'_{ion-elec}(\vec{r}) - \hat{V}_{ion-elec}(\vec{r}) | \psi \rangle - \langle \psi' | \hat{V}'_{ion-elec}(\vec{r}) - \hat{V}_{ion-elec}(\vec{r}) | \psi' \rangle \quad (2.10)$$

If the both $\hat{V}_{ion-elec}(\vec{r})$ and $\hat{V}'_{ion-elec}(\vec{r})$ gave the same electron density $n(r)$, the two terms on the right-hand side of Eq 2.10 would be expressed by

$$\langle \psi | \hat{V}'_{ion-elec}(\vec{r}) - \hat{V}_{ion-elec}(\vec{r}) | \psi \rangle = \int (V'_{ion-elec}(\vec{r}) - V_{ion-elec}(\vec{r})) n(\vec{r}) d\vec{r} \quad (2.11)$$

and

$$\langle \psi' | \hat{V}_{ion-elec}(\vec{r}) - \hat{V}'_{ion-elec}(\vec{r}) | \psi' \rangle = \int (V_{ion-elec}(\vec{r}) - V'_{ion-elec}(\vec{r})) n(\vec{r}) d\vec{r} \quad (2.12)$$

Eqs. 2.10, 2.11, and 2.12 lead to the contradictory relation $(E + E') < (E + E')$. Therefore, our assumption that $n(r)$ is the same with the different external potentials is not correct.

Thus there is one-to-one correspondence between electron density and external potential

This proves the Hohenberg-Kohn theorem

But the question remains why density and not wavefunction? the answer to this question lies in the fact as the number of particles increases the number of variables required to define wavefunction also increases whereas for any number of particles, the density always remains the function of 3 spatial variables. This allows solving the same problem with lower computational cost and lower storage required to store the vital information about the system.

Hence we can write

$$E[n(\vec{r})] = \langle \psi | \hat{H} | \psi \rangle = \langle \psi | \hat{G}[\hat{n}(\vec{r})] | \psi \rangle + \int d\vec{r} V_{ion-elec}(\vec{r}) n(\vec{r}) \quad (2.13)$$

2.2.2 2nd Hohenberg-Kohn Theorem

The 2nd Hohenberg-Kohn Theorem states that If the functional $\hat{G}[\hat{n}(\vec{r})]$ was known, then by minimizing the total energy in Eq 2.13, with respect to variations in the electron density $n(\vec{r})$, the ground state of the electron density and the total energy is obtained.

Using Hellmann Feynman Theorem and variational principle:

$$\begin{aligned} \frac{dE[n(\vec{r})]}{dn(\vec{r})} &= \langle \psi | \frac{d\hat{H}}{dn(\vec{r})} | \psi \rangle \\ &= \langle \psi | \frac{\hat{G}\hat{n}(\vec{r})}{dn(\vec{r})} | \psi \rangle + \frac{d}{dn(\vec{r})} \int d\vec{r} V_{ion-elec}(\vec{r}) n(\vec{r}) \\ &= 0 \end{aligned} \quad (2.14)$$

We have to use the variational principle under the constraint that $\int n(\vec{r}) d\vec{r} = N$, where N is the total number of electrons in the system.

2.3 Kohn-Sham Equations

Before diving into fundamental equations governing DFT. We will focus our attention on total energy and the terms involved in it. We refer back to Eq.2.13 and try to explain the term $\langle \psi | \hat{G}[\hat{n}(\vec{r})] | \psi \rangle$.

$$\langle \psi | \hat{G}[\hat{n}(\vec{r})] | \psi \rangle = \langle \psi | \hat{T}[\hat{n}(\vec{r})] | \psi \rangle + \langle \psi | \frac{1}{r-r'} | \psi \rangle \quad (2.15)$$

First, we look at the second term on the right-hand side in the above equation i.e. $\langle \psi | \frac{1}{r-r'} | \psi \rangle$.

$$\langle \psi | \frac{1}{r-r'} | \psi \rangle = \frac{1}{2} \int \frac{n(\vec{r})n(\vec{r}')}{|r-r'|} + E_{xc}[n(\vec{r})] \quad (2.16)$$

The first term in the Eq. 2.16 is Hartree potential energy. This term represents Coulombic repulsion felt by electrons due to other electrons. Whereas $E_{xc}[n(\vec{r})]$ is exchange-correlation energy. Both these terms together show the complete picture of the inter-electronic interactions in molecules and solids. We will further look into these terms in the next section.

The first term on the right-hand side is the Kinetic energy term. The form of Kinetic energy term with respective density was proposed by Kohn Sham.

Now let us shift our focus to the Kohn-Sham equation

$$\begin{aligned} \frac{dE[n(\vec{r})]}{dn(\vec{r})} &= \sum_{i=1}^N \frac{d}{dn(\vec{r})} \left\langle \psi \left| \frac{-\nabla^2}{2} \right| \psi \right\rangle + \frac{1}{2} \frac{d}{dn(\vec{r})} \int \frac{n(\vec{r})n(\vec{r}')}{|r-r'|} \\ &+ \frac{d}{dn(\vec{r})} \int d\vec{r}' V_{ion-elec}(\vec{r})n(\vec{r}) + \frac{dE_{xc}[n(\vec{r})]}{dn(\vec{r})} \end{aligned} \quad (2.17)$$

Where electron density is given by $n(\vec{r}) = \sum_{i=1}^N |\psi(\vec{r})|^2$. Now solving Eq. 2.17 using Variational principle with constraint that $\int n(\vec{r}) d\vec{r} = N$. we get set equations that are similar to single particle Schrodinger equation given by

$$\left[\frac{-\nabla^2}{2} + V_{eff} \right] \psi_i^{KS} = \epsilon_i \psi_i^{KS} \quad (2.18)$$

where V_{eff} is given by

$$V_{eff}[n(\vec{r})] = V_{ion-elec}(\vec{r}) + \int \frac{n(\vec{r}')}{|r-r'|} dr' + \frac{dE_{xc}[n(\vec{r})]}{dn(\vec{r})} \quad (2.19)$$

where the second term on the right-hand side is Hartree potential and the third term is exchange-correlation potential.

$$V_{xc}[n(\vec{r})] = \frac{dE_{xc}[n(\vec{r})]}{dn(\vec{r})} \quad (2.20)$$

Now assuming we know the form of $V_{xc}[n(\vec{r})]$ we can solve these Kohn Sham equations iteratively using the Self-Consistent Field (SCF) method.

2.4 Approximations

2.4.1 Exchange-Correlation Functional

The unknown part in the Kohn Sham Hamiltonian is the Exchange-Correlation (XC) functional. The kinetic energy expectation value was obtained using formalism which is similar to that used in Hartree Fock hence the interacting nature of the kinetic energy term is missing. Also, the Hartree term only accounts for coulomb repulsion, so other exchange and correlational effects present between in the electron are missing. All these missing effects are taken into account by the XC functional.

The only catch is that we don't know the exact functional form of XC functional. It was stated by the Hohenberg-Kohn theorems that this exact functional form does exist but not knowing the functional form of XC functional makes it impossible to solve the Kohn sham equations.

Local Density Approximation (LDA)

The LDA is an approximation based on the uniform-electron system. The contribution of exchange interaction to the total energy for the uniform-electron charge is given by:

$$E_x[n] = NC_2n^{1/3} \quad (2.21)$$

Now, let us consider Eq. (2.21) for the case of the non-uniform-electron charge, in which n is a function of \vec{r} . If $n(\vec{r})$ slowly varying function, the exchange functional $E_x[n(\vec{r})]$ is approximated as

$$E_x[n(\vec{r})] \approx NC_2n^{1/3} \quad (2.22)$$

where N can be written as $\int n(\vec{r}) d\vec{r} = N$, therefor Eq. (2.22) becomes

$$E_x[n(\vec{r})] = \int \epsilon_x(\vec{r})n(\vec{r}) d\vec{r} \quad (2.23)$$

Where ϵ_x is given by

$$\epsilon_x = C_2n^{1/3} \quad (2.24)$$

Since Eq. (2.23) is based on the free-electron gas, the correlation interaction is needed to capture accurately the many-body system. Therefore, the energy of correlation interaction

$\epsilon_c(\vec{r})$ is added to Eq. (2.23) as

$$E_x[n(\vec{r})] = \int [\epsilon_x(\vec{r}) + \epsilon_c(\vec{r})]n(\vec{r}) d\vec{r} \quad (2.25)$$

This is a general expression for **Local Density Approximation** for XC functional. The expression for $\epsilon_c(\vec{r})$ was calculated using low density [5] and high-density limit [6]. The more accurate numerical calculation of $\epsilon_c(\vec{r})$ is given by Ceperley and Alder [7]. They calculated the total energy for the uniform-electron system for different values of r_s by using the quantum Monte Carlo method. Then the correlation energy was obtained by subtracting the corresponding kinetic and exchange energies from the total energy. Based on fitting functions to the numerical results of Ceperley and Alder, several forms of $\epsilon_c(\vec{r})$ are proposed by Vosko, Wilk, and Nusair (VWN) [8], Perdew and Zunger (PZ) [9], and Perdew and Wang (PW) [10].

Generalised Gradient Approximation (GGA)

The LDA is an approximation in the case that $n(\vec{r})$ is a slowly varying function. However, $n(\vec{r})$ often changes rapidly in the real material. Moreover, $n(\vec{r})$ is generally spin-dependent. There are many attempts to improve the accuracy of the LDA for real systems where $n(\vec{r})$ varies rapidly. The most successful one is the **Generalized Gradient Approximation** (GGA). In the GGA, for the exchange term, an enhancement factor F_X is added in Eq. (2.23) by Perdew, Burke, and Ernzerhof (PBE) [11] as

$$\begin{aligned} E_x[n(\vec{r})] &= \int \epsilon_x(\vec{r})n(\vec{r})F_x(s) d\vec{r} \\ &= C_2 \int n^{4/3}(\vec{r})F_x(s) d\vec{r} \end{aligned} \quad (2.26)$$

where s is the dimensionless gradient of $n(\vec{r})$, which is defined by

$$s = \frac{|\nabla n(\vec{r})|}{2k_F n(\vec{r})} \quad (2.27)$$

where $k_f = [3\pi^2 n(\vec{r})]^{1/3}$ and the enhancement factor $F_X(s)$ is expressed as

$$F_X(s) = 1 + \kappa - \frac{\kappa}{1 + \mu s^2 / \kappa} \quad (2.28)$$

Also for the correlation term $E_c[n(\vec{r})]$ is expressed by $\epsilon_c(\vec{r})$ of the uniform electron system plus an additional term $H[n(\vec{r}), \zeta]$ which depends on both the gradient $\nabla n(\vec{r})$ and the spin polarization ζ . The $E_c[n(\vec{r})]$ functional is given by PBE as

$$E_c[n(\vec{r})] = \int [\epsilon_c(\vec{r}) + H[n(\vec{r}), \zeta]n(\vec{r}) d\vec{r} \quad (2.29)$$

Therefore $E_{xc}[n(\vec{r})]$ can be written as

$$E_c[n(\vec{r})] = \int [C_2 n^{4/3}(\vec{r})F_x(s) + \epsilon_c(\vec{r}) + H[n(\vec{r}), \zeta]n(\vec{r}) d\vec{r} \quad (2.30)$$

This is a general expression for **Generalized Gradient Approximation** for XC functional.

2.4.2 Pseudopotentials

Pseudopotential is the most widely used approximation in any electronic structure calculation method. The approximation is generally used in order to minimize the computational cost required to solve the many-body Hamiltonian. In this approximation, the all-electron potential due core states of the atom is replaced by an effective potential, and the valence state wavefunctions are smoothed out near the core.

The approximation helps in tackling the problem of usage of a large number basis to represent the states as we go near the core region. This is because, near the core region, the electronic wavefunction becomes highly oscillatory this is due to the fact the probability of finding an electron becomes large as we near the core due to the strong coulomb attraction of the nucleus. Therefore the pseudopotentials are useful to to carry out faster electronic calculations because they reduce the number basis required by replacing the strong coulombic potential with an effective potential and its effect on the valence states are smoothed.

The two main properties of pseudopotentials are;

1. **Transferability**: Transferability is properties in which a pseudopotential can be used to represent atoms in different chemical environments.
2. **Smoothness (softness)**: The degree at which the valence electron wavefunction is smoothed out in the core region. This depends type of properties that one is

interested in studying.

There are 3 types of widely used pseudopotentials **Norm Conserving** (NC), **Ultra Soft** (US), and **Projector Augmented Wave** (PAW). We discuss each of these pseudopotentials in brief.

1. **Norm Conserving** (NC): In norm-conserving NC, the core states are replaced by the effective potential, and the valence electron wavefunctions are smoothed near the core up to some radial grid value known as r_{cut} value. The additional condition in NC is that the norm of the valence electron wavefunction within a certain radius should match the norm in the All-Electron (AE) calculation. This means NC does need a high number of bases compared to other pseudopotential types which increases the time taken for computation.
2. **Ultra Soft** (US): The ultra-soft pseudopotentials relax the condition of the norm conservation to a degree and focus on smoothness. This means ultra soft are less accurate but are faster.
3. **Projector Augmented Wave** (PAW): The PAW approach utilizes projector functions to separate core and valence electron wavefunctions. It avoids explicitly including core electrons in the calculations. However, it ensures the valence electron wavefunctions match the all-electron wavefunctions beyond a core radius, similar to NCPPs. Hence PAW provides a balance between transferability (like NC) and smoothness (like US).

Below is an example of PAW type pseudopotential for Molybdenum.

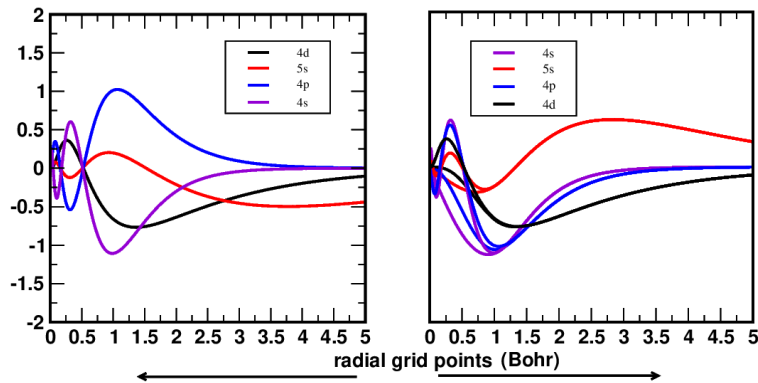


Figure 2.1: Plot shows all electron valence wavefunctions (left) and pseudized valence wavefunction (right)

2.5 Plane wave method

The electronic structure suite that was utilized for this particular project is known as Quantum Espresso, as described in [12]. The basis set employed by Quantum Espresso for representing Kohn-Sham wavefunctions (orbitals) is plane waves. Although there are various options when it comes to the choice of basis for representing KS wavefunction, for solids, using a plane wave basis can be directly related to the formalism of solids in band theory.

According to Bloch's theorem, due to the periodicity of translation in solids, the electronic wave function in solids should also obey this periodicity. As a result, electronic wavefunctions should be eigenfunctions of the translation operator.

$$\hat{T} \Psi_k^n(\vec{r}) = \Psi_k^n(\vec{r} + \vec{a}) = u_k^n(\vec{r}) \Psi_k^n(\vec{r}) \quad (2.31)$$

The solution for this scenario is plane waves. A KS wavefunction can be written.

$$\Psi_k^n(\vec{r}) = \sum_G C_G^{n,k} e^{i(\vec{G} + \vec{k}) \cdot \vec{r}} \quad (2.32)$$

Where the vector \vec{G} are called reciprocal lattice vectors and $C_G^{n,k}$ are the coefficient, to be determined.

All eigenstates Ψ_k^n that have the same \vec{k} but different n expand with the same k basis functions. For the eigenstates of another \vec{k} uses a new basis function of the new \vec{k} ; Thus n here represents the band index.

2.6 Self Consistent Field method

Despite the simplicity of the formalism of Density Functional Theory (DFT), solving a many-body Hamiltonian is not easy. The density is given as $n(\vec{r}) = \sum_{i=1}^N \psi_i^{KS}(\vec{r})$, and there is interdependence between KS orbitals and density, as explained in Equation (2.17). To solve this issue, Kohn and Sham proposed using the Self Consistent Field (SCF) method in DFT[13].

1. **Initial Guess:** The SCF method starts with an initial guess for the electron density (distribution of electrons in space).

2. **Building the Potential:** Based on the initial guess, an effective potential (often including terms for the interaction between electrons and the nucleus, and between electrons themselves) is constructed. .

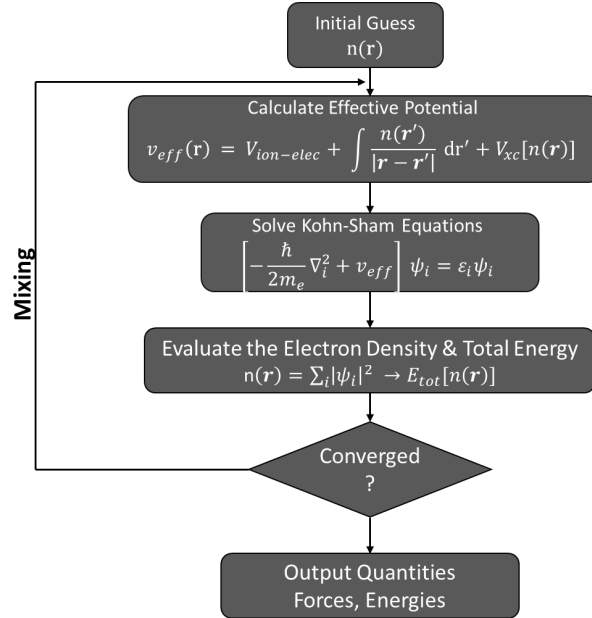


Figure 2.2: Self Consistent field (SCF) Loop for the

3. **Solving the Kohn-Sham Equation:** Using the effective potential, the Kohn-Sham equation (which governs the behavior of electrons) is solved for the one-electron KS wavefunctions (orbitals) of the system.
4. **Recalculating the Density:** From the obtained wavefunctions, a new electron density is calculated.
5. **Iteration and Convergence:** This is where the "self-consistent" part comes in. The newly calculated density is compared to the initial guess. If they are not the same, the process repeats from step 2 using the new density as the guess or by mixing the old and new density. This iterative process continues until the calculated density and the density used to generate the potential become consistent (converge).

The SCF method was implemented using `pw.x` executable of **Quantum espresso** . Which gives converged charge density and total energy of the system.

2.7 Structural Optimization

The energy of a crystal is determined by the positions of its atoms or ions and the electrons that surround them. In other words, the total energy of the crystal is a function of its atomic and ionic configuration, represented mathematically as $E(R_i)$. Therefore, the equilibrium energy of the crystal is influenced by the positions of its atoms. The expression for this equilibrium energy is given as:

$$F_i = -\nabla_{R_i} E(R_i) \quad (2.33)$$

It tends to zero as the system reaches its equilibrium configuration. Now if $E(R_1, \dots, R_n)$ of a crystal structure depends on the parameters R_1, R_2, \dots, R_n . Then the equilibrium structural parameter R_m is the value of R at which $E(R_{min}) = E_{min}$. It implies the first derivative concerning R at R_m must be equal to zero.

$$\left(\frac{\partial E}{\partial R} \right)_{R_{min}} = 0 \quad (2.34)$$

In consequence, given the DFT calculated total energy $E[n(r)]$, the external pressure on the unit cell is calculated as follows,

$$P = -\frac{\partial E}{\partial V} \quad (2.35)$$

The system will be in equilibrium when the pressure P becomes zero.

There are 3 types of relaxations:

1. **Volume relaxation:** In this, the total energy is minimized w.r.t volume.
2. **External relaxation:** Here the total energy is minimized w.r.t to unit cell (unit cell vectors).
3. **Internal relaxation:** In this, the total energy energy is minimized w.r.t to atomic position in unit cell.

Using Quantum espresso suite's `pw.x` executable we can also perform **Internal relaxation** (using `relax calculation`) and **Volume relaxation** and **Internal relaxation** (using `vc-relax relaxation`).

2.8 Band Structure

When electrons are present in solids, their movement is affected by the proximity of neighboring atoms and their nuclei, leading to restricted and unique electronic structures. The band theory, based on Bloch's theorem, elucidates the influence of these interactions on the formation of allowed energy bands, separated by forbidden energy gaps, and determines the electronic properties of materials, such as whether they are metals, insulators, or semiconductors.

Quantum Espresso software is a widely used open-source tool for electronic structure calculations and materials modeling. Specifically, the '**pw.x**' executable is utilized for **Self-Consistent field (SCF)** calculations, which provide the ground-state energy and charge density of a given system. During the SCF calculation, the '**pw.x**' executable constructs a Hamiltonian matrix that calculates Kohn-Sham wavefunctions and their eigenvalues, exclusively for valence states. The results are saved in the '**pwscf.save** (prefix.save)' folder, for further use.

To calculate bands in the conduction level, a non-self-consistent field (SCF) calculation is necessary. This involves utilizing the charge density that has been converged from the SCF calculation. The calculation is then set as bands in '**pw.x**' executable, and the remaining process is identical to the calculation of bands for valence levels.. The data generated is then saved as '**pwscf.wfc**' binary files. Visualization of the calculated band structure is achieved through the use of the '**bands.x**' post-processing executable. This program converts band data from the '**pwscf.wfc**' folder and generates a plot of the band structure in various formats, such as **.gnu** or **.xmgr**, which can be further analyzed using external software.

For the present work, band structure diagrams were plotted using **Xmgrace** software.

2.9 Density of states

The density of states (DOS) describes the number of electron states allowed per unit of energy and volume. High DOS at a certain energy level means many available states for electrons at that same level. Conversely, low DOS means fewer available states.

In Quantum espresso, the density of states calculation is performed after the **SCF** calculation using the '**pw.x**' executable. Once the **SCF** calculation is complete, a **non-**

SCF calculation is performed to generate 'pwscf.wfc' files. These files are then converted into .gnu or .xmgr formats using dos.x.

Partial density of states (PDOS)

The partial density of states is a tool used to determine how each element present in a molecule contributes to the total density of states of molecules in different structures. This tool calculates the partial density of states using atomic wavefunctions of that particular atom, and thus it gives insight into which orbital of a particular atom contributes how much to the density of states (DOS).

To obtain the PDOS, one needs to use the 'projwfc.x' post-processing tool. This tool creates .xmgr or .gnu files for each atom, which can then be used to plot the partial density of states.

2.10 vdW functionals

In this project, we are using DFT-D and non-local functionals to incorporate vdW interactions in DFT.

1. **DFT-D:** It is a well-established fact that van der Waals (vdW) energy can be modeled using a damped inter-atomic potential that is directly proportional to $1/R^6$, where R represents the inter-atomic distance. Therefore, a straightforward approach is to include an energy term with $1/R^6$ in the total energy calculation.

$$E_{DFT-D} = E_{DFT} + E_{vdW} \quad (2.36)$$

where E_{vdW} denotes the vdW energy, E_{vdW} is given by

$$E_{vdW} = -\frac{s_6}{2} \sum_{I \neq J} \frac{C_6^{IJ}}{R_{IJ}^6} f_d(R_{IJ}) \quad (2.37)$$

here s_6 is a global scaling factor depending on the specific GGA and C_6^{IJ} denotes the dispersion coefficient for atom pair IJ . The C_6^{IJ} coefficients are taken by a least-square fitting procedure from the work of Wu and Yang [14]. $f_d(R_{IJ})$ is a

damping function, which is given by [3]:

$$f_d(R_{IJ}) = \frac{1}{1 + e^{-d(R_{IJ}/R_r - 1)}} \quad (2.38)$$

here the parameters d and R_r are fitted to experimental or accurate theoretical data. The DFT-D method is an inexpensive and straightforward calculation, but it is not a fully first-principles approach. Examples. Grimme df2 [3] and Grimme df3 [15].

2. **Nonlocal vdW functionals:** This method replaces the vdW energy term E_{vdW} in Eq 2.36 by non-local (nl) energy functional of the electron density $n(\vec{r})$, which is given as six-dimensional integral.

$$E_{vdW}^{nl}[n(\vec{r})] = \frac{1}{2} \int \int n(\vec{r}) \Phi(\vec{r}, \vec{r}') n(\vec{r}') d\vec{r} d\vec{r}' \quad (2.39)$$

where $\Phi(\vec{r}, \vec{r}')$ is a function depending on $r - r'$ and the densities n in the vicinity of r and r' [16]. Several non-local vdW functionals have been proposed, such as vdW-DF [16], [17], vdW-DF2 [18], vdW-DF3-opt1 [19], vdW-DF3-opt2 [19], vdW-DF- C6 [20], or rVV10 [21].

Chapter 3

Results

3.1 Brief

MoS₂ belongs to a class of materials called Transition Metal Dichalcogenides (TMDCs). This chapter studies structural and electronic properties of the monolayer, bilayer, and bulk MoS₂ structure. Also, the dependence of interlayer distance on the Band structure of the bilayer MoS₂ is studied.

3.2 Monolayer

The monolayer MoS₂ is 2D Van der Waals material, derived from its bulk structure which has a hexagonal bravais lattice. It has a Metal (Mo) layer sandwich between layers of two non-metal elements (S).

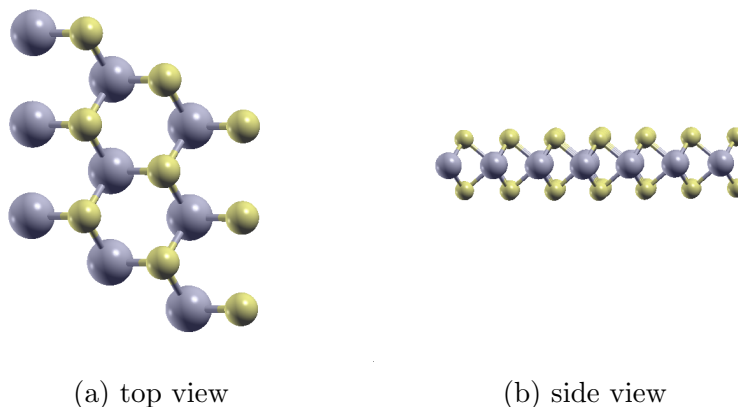


Figure 3.1: This figure shows a visualization of MoS₂ monolayer from top and side.

3.2.1 Convergence tests

When performing DFT calculation we need to find the convergence of total energy of the system w.r.t to maximum allowed kinetic energy for wavefunctions (number of plane waves used), w.r.t to k point grid used for the Brillouin zone integration and sometimes also w.r.t to kinetic energy cutoff (Ry) for charge density and potential. The optimization helps us to reduce computational cost and assure accuracy in the obtained results.

In the below figure convergence of total energy w.r.t to $E_{\text{cut-wfc}}$ i.e. maximum allowed kinetic energy for wavefunctions was performed. The K-point mesh was set to $4 \times 4 \times 1$ for this calculation.

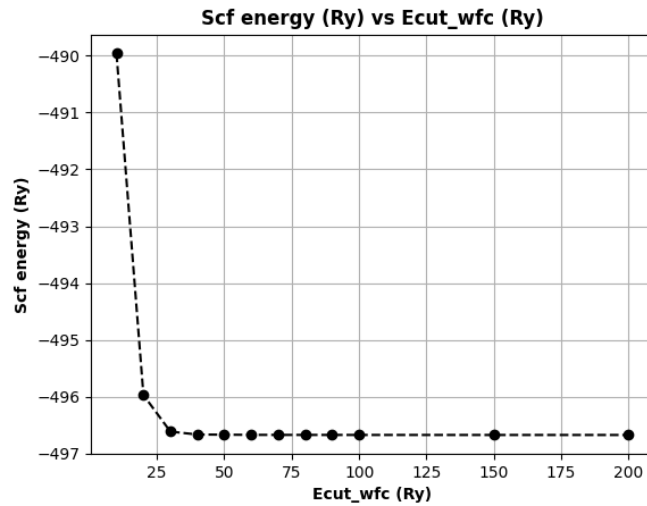


Figure 3.2: Above figure shows plot of SCF energy w.r.t kinetic energy cut off both in units of Ry.

In Fig 3.2 it can be seen that after 30 Ry of Kinetic energy total energy of the system converges. Thus we can conclude from these that around 40-50 Ry value of $E_{\text{cut-wfc}}$ assures good accuracy for the calculations.

As shown in Fig. 3.3, we performed convergence of total energy w.r.t to K point mesh used for the Brillouin zone integration. For this calculation, the $E_{\text{cut-wfc}}$ was set to 60 Ry. The k-point values were varied from 16 to 196. In this fig, it can be seen that as the number of K points increases the variation in the total energy goes to almost zero. This indicates a proper convergence has been achieved. The optimum value of K points is 64 or $8 \times 8 \times 1$. For subsequent calculations, this optimized value of $E_{\text{cut-wfc}}$ and K points will be used (Unless explicitly mentioned).

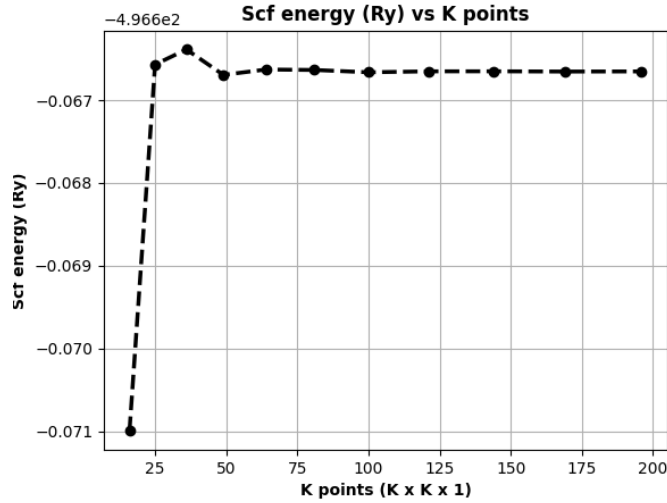


Figure 3.3: Above figure shows the plot of SCF energy w.r.t discretized k vector (or k-points) grid.

3.2.2 Volume Optimization

Volume optimization of monolayer MoS₂ was performed. The structure's volume was optimized to get its in-plane lattice parameter. PAW-type pseudopotential was used for the optimization and results were compared with their experimental values $a = 3.16 \text{ \AA}$ [22].

It can be seen from Fig 3.4 that the total energy attains a minimum value at around 3.18 \AA . Thus DFT calculated in-plane lattice parameter for the monolayer is 3.18 \AA which is a relative percentage error of 0.6 %.

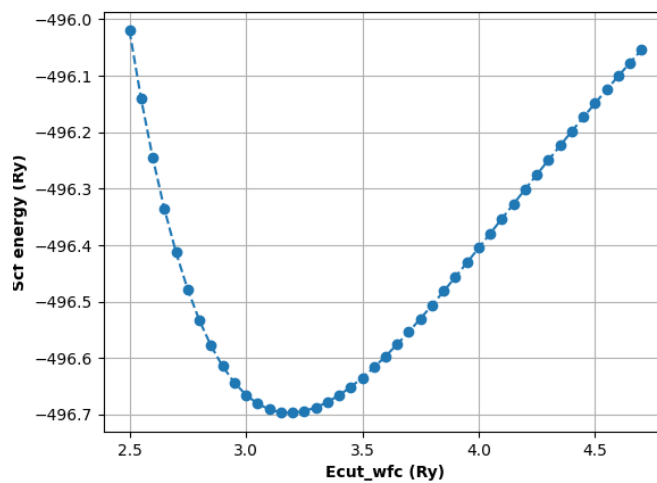


Figure 3.4: Above figure shows plot of SCF energy w.r.t lattice constant in Ang done with GGA exchange-correlation using PAW pseudopotential

3.2.3 Electronic Properties

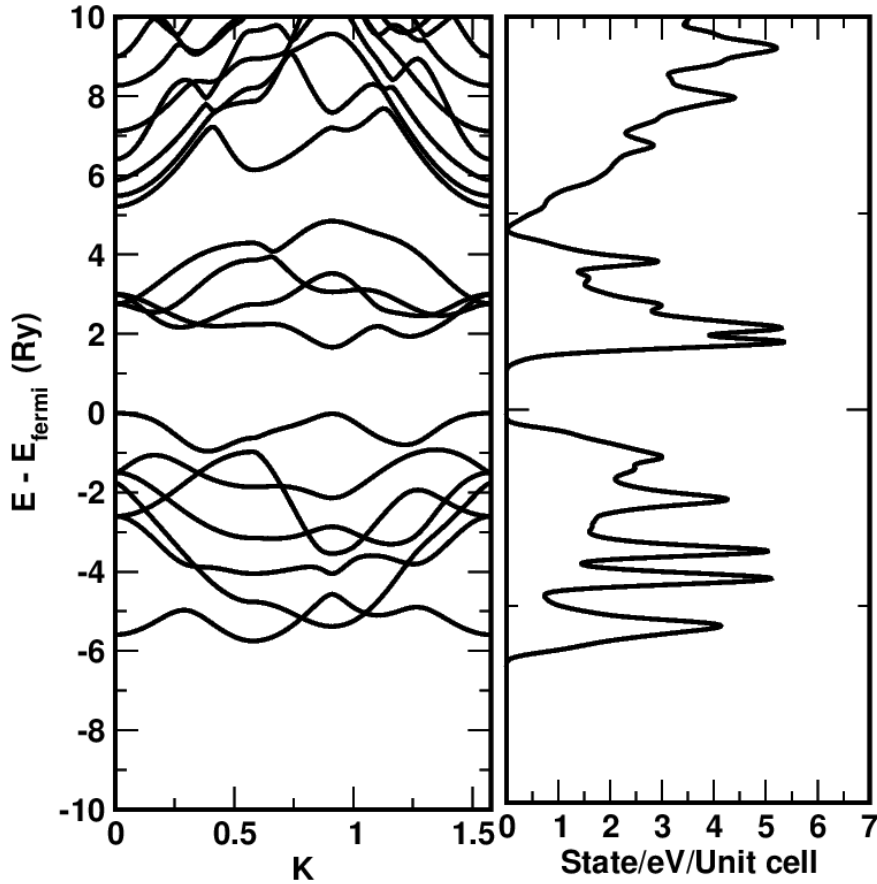


Figure 3.5: Above figure shows plot of electron dispersion curve and TDOS of MoS_2

The above figure shows band structure and total density of states of MoS_2 monolayer. It shows band gap of 1.6765 eV. This band gap is obtained using PAW type pseudopotential and using GGA as XC-functional. The monolayer band structure shows direct transition

	Band Gap
Experimental value	1.90 eV
Theoretical value	1.6765 eV

Table 3.1: Table showing Experimental value and Theoretical value of Bandgap for MoS_2

at K high symmetry point with experimental band gap value of 1.8 - 1.90 eV [1]. It was also observed that LDA type XC-functional gives a bandgap around 1.78 eV, which is closer to the value obtained using GGA type XC-functional.

The total density of states also shows a bandgap of around 1.67 eV. The slight inconsistency in TDOS and Band structure graph is due to the tetrahedron method which estimates a little higher fermi energy compared to fermi energy we get after doing SCF.

This inconsistency can be resolved using better methods such as the optimized tetrahedron method.

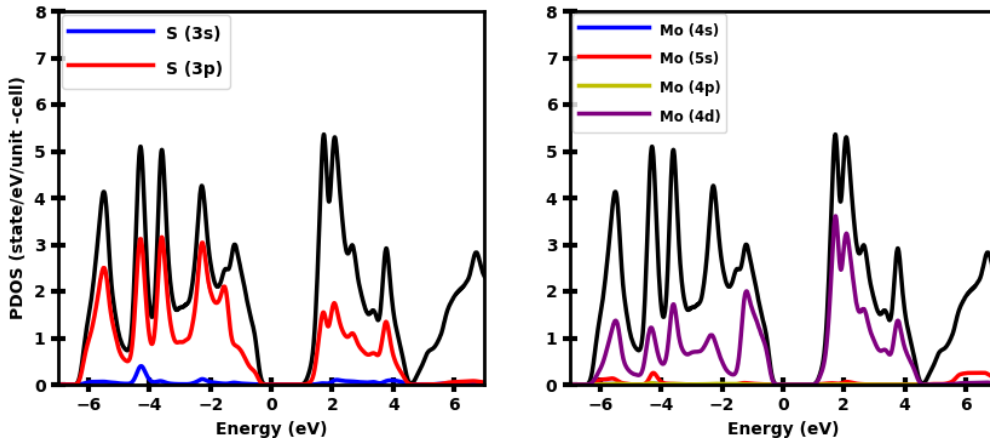


Figure 3.6: Above figure shows the plot of TDOS and PDOS (Left) PDOS of sulfur (Right) PDOS of Molybdenum

Also, plots of contributions of the individual atomic density of states or partial density of states to the total density of states were studied for sulfur atoms (S) and molybdenum atoms (Mo). As seen in fig 3.6 it is clear in the case of S the 3p contribution is higher than 3s where $3s^23p^4$ is the valence orbitals. Whereas in the case of Mo, the contribution from the 4d is higher compared to other orbitals where its valence orbitals are $5s^14d^5$. This is because the bonding occurs between atoms because of Mo's 4d and S's 3p as they have the highest free electron density. Hence their contributions to the total density of states of states are much higher than other orbitals.

3.2.4 Spin Orbit Coupling

The introduction of the spin-orbit coupling in the monolayer is done by using fully relativistic calculations done by PAW-type pseudopotentials. It is seen that there is a significant splitting of the valence band at the K high symmetry point. The difference in energy of split bands at K is $\Delta E_{SOC} = 0.144eV$ which is consistent with the experimental value of 0.1 eV [23].

The valence band splitting in single-layer MoS_2 is primarily attributed to the presence of spin-orbit coupling (SOC). In single-layer MoS_2 , the lack of inversion symmetry leads to a significant spin-orbit splitting, which breaks the degeneracy of the valence band maximum along the direction -K. This strong spin-orbit coupling results in the separation

of spin-up and spin-down states in the valence band, creating a sizable energy splitting between the two spin states.

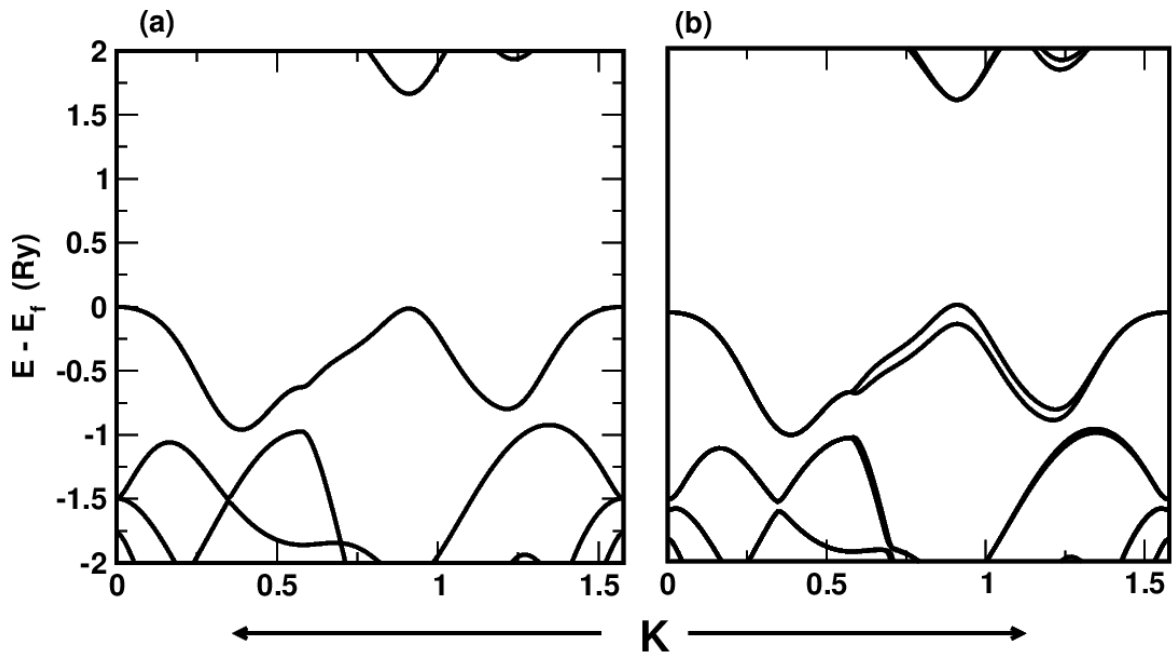


Figure 3.7: Above figure shows the plot of spin-orbit coupling in monolayer MoS₂, (a) Without spin-orbit coupling (b) with spin-orbit coupling.

3.3 Bilayer

3.3.1 Convergence tests

Similar to monolayer, convergence tests were performed for convergence of total energy of the system w.r.t to maximum allowed kinetic energy for wavefunctions (number of plane waves used), w.r.t to k point grid used for the Brillouin zone integration and sometimes also w.r.t to kinetic energy cutoff (Ry) for charge density and potential. The optimization helps us to reduce computational cost and get good accuracy in our results.

In the below figure convergence of total energy w.r.t to Ecut-wfc i.e. maximum allowed kinetic energy for wavefunctions was performed. The Kpoint mesh was set to 4 X 4 X 1 for this calculation.

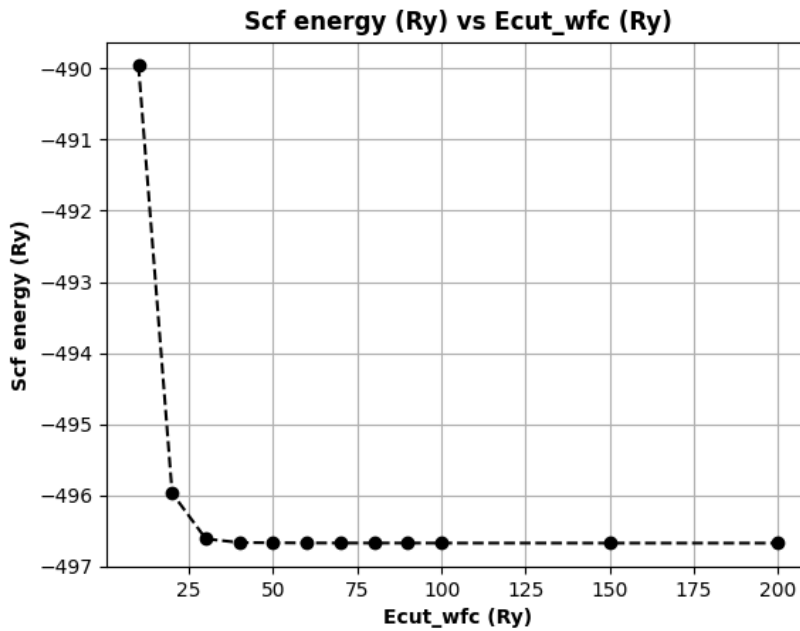


Figure 3.8: Above figure shows plot of SCF energy w.r.t kinetic energy cut off both in units of Ry.

In Fig 3.12 it can be seen that at a certain value of Kinetic energy cut off for wavefunctions the total energy of the system converges. Thus we can conclude from these that around 40-50 Ry value of Ecut-wfc is the optimum value to get good accuracy in the total energy of the system.

We also performed convergence of total energy w.r.t to K point mesh used for the Brillouin zone integration. For this calculation, the Ecut-wfc was set to 60 Ry. The k-point values were varied from 16 to 196. In this fig, it can be seen that as the number

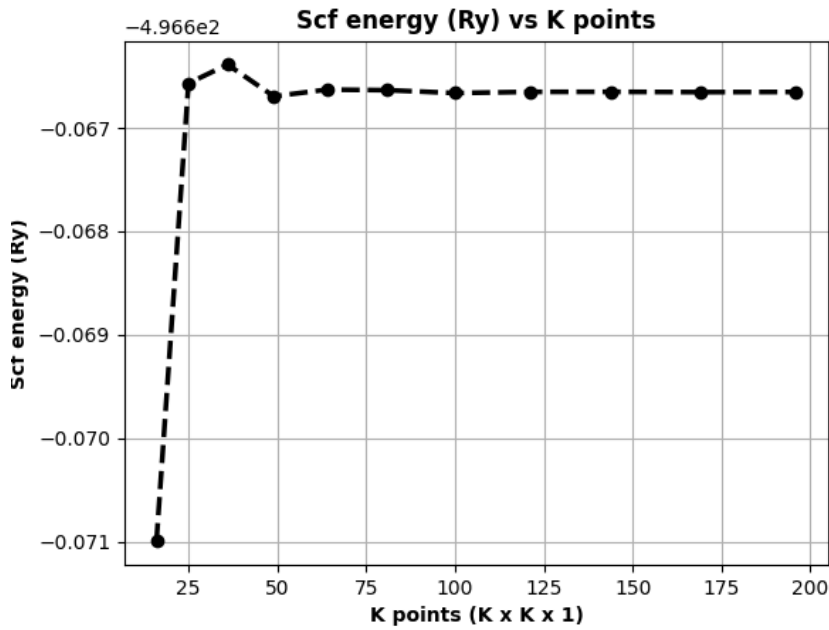


Figure 3.9: Above figure shows the plot of SCF energy w.r.t discretized k vector (or k-points) grid.

of K points increases the variation in the total energy goes to almost zero. This indicates a proper convergence has been achieved. The optimum value of K points is 64 or 8 X 8 X 1. For subsequent calculations, this optimized value of Ecut-wfc and K points will be used (Unless explicitly mentioned).

3.3.2 Volume Optimization

The volume optimization was done to relax the bilayer structure, and 7 exchange functionals were used for volume optimization. By relaxing the bilayer we obtained an in-plane lattice constant and the interlayer distance between two layers. The experimental values

XC-functional	lattice constant - a	Interlayer spacing - d
GGA	3.1854	7.4100
LDA	3.1236	6.0349
vdw-df-c6	3.16759	6.1491
vdw-df3-opt1	3.15654	6.1358
vdw-df3-opt2	3.1632	6.1459
grimme-df2	3.1908	6.2129
grimme-df3	3.1858	7.2132

Table 3.2: The above table shows optimized in-plane constant-a and interlayer distance value using different types of XC functionals in \AA unit.

for in-plane lattice constant remain the same as that in the case of monolayer i.e. 3.16 Å [22]. The interlayer distance experimental value is around 6.15 Å. It can be seen from the table that vdw non-local functionals give a better estimate of interlayer distance with a percentage error of 0.02 %. GGA overestimates both lattice constant as well as interlayer spacing whereas LDA underestimates the same. The Grimme-*df2* and Grimme-*df3* DFT-D methods give almost the same results as that of GGA.

3.3.3 Electronic Properties

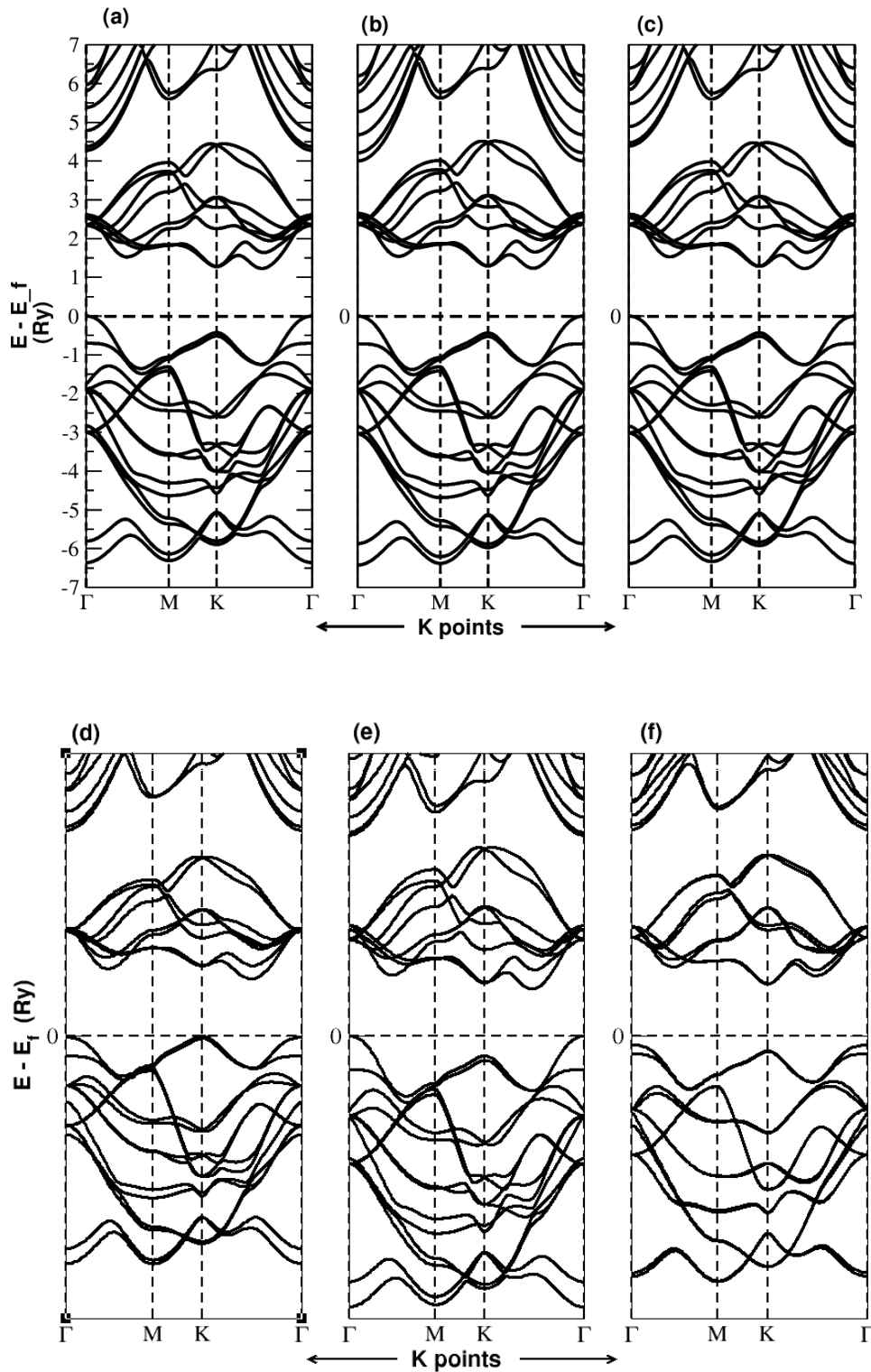


Figure 3.10: Above figure shows plot of electron dispersion curves of MoS₂, a) Band structure obtained using vdw-df-C6 b) Band structure obtained using vdw-df3-opt1 c) Band structure obtained using vdw-df3-opt2 d) Band structure obtained using Grimme-df2 e) Band structure obtained using LDA f) Band structure obtained using GGA.

The above figure shows band structure of MoS₂ bilayer. This band gap is obtained using PAW type pseudopotential and using 6 different XC-functional. It shows different band gap values depending on the type of XC-functional used for the calculation.

XC-functional	Experimental Band Gap	Band Gap obtained
vdw-df-C6	1.53 eV	1.2262 eV
vdw-df3-opt1	1.53 eV	1.2332 eV
vdw-df3-opt2	1.53 eV	1.2270 eV
grimme-df2	1.53 eV	1.4479 eV
LDA	1.53 eV	1.1651 eV
GGA	1.53 eV	1.5196 eV

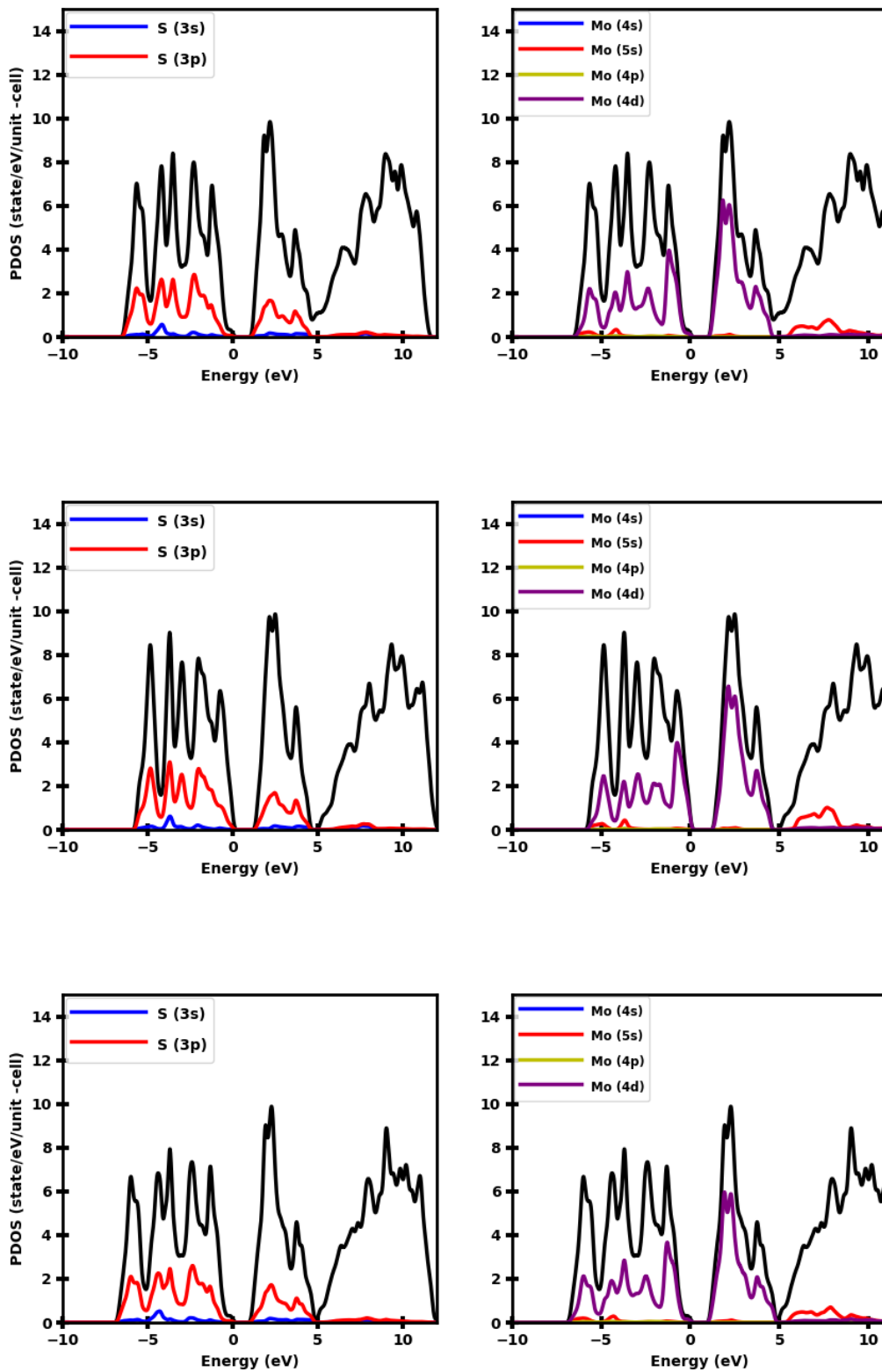
Table 3.3: Table showing Experimental value and Theoretical value of Bandgap for MoS₂ bilayer for different XC-functional

Unlike monolayer, the band structure of bilayer MoS₂ shows an indirect transition from Γ to between K- Γ high symmetry points with an experimentally obtained bandgap of 1.53 eV [2]. This nature is observed in all XC-functional except in GGA, and Grimme df methods. The GGA shows the transition from K to Γ high symmetry point. The reason for this different nature for GGA and Grimme df is due to their inconsistency in producing accurate interlayer distance. This also shows that to get the proper nature of band structure in case bilayer the interlayer spacing plays a major role.

The band structure values produced by all XC-functional are not that accurate and have huge deviation from the experimental value showing 19-20 % relative percentage error. This shows although some functional quite accurately describe the nature of band structure still most of them fail to produce an accurate value.

Also, plots of contributions of the individual atomic density of states or partial density of states to the total density of states were studied for sulfur atoms (S) and molybdenum atom (Mo). The density of states calculation were done using the tetrahedron method. For this dense k-point grid was used i.e. 48 X 48 X 1 for proper sampling of the Brillouin zone.

Below are the plots for non-local functionals, Grimme df, LDA, and GGA produced using PAW type pseudopotential.



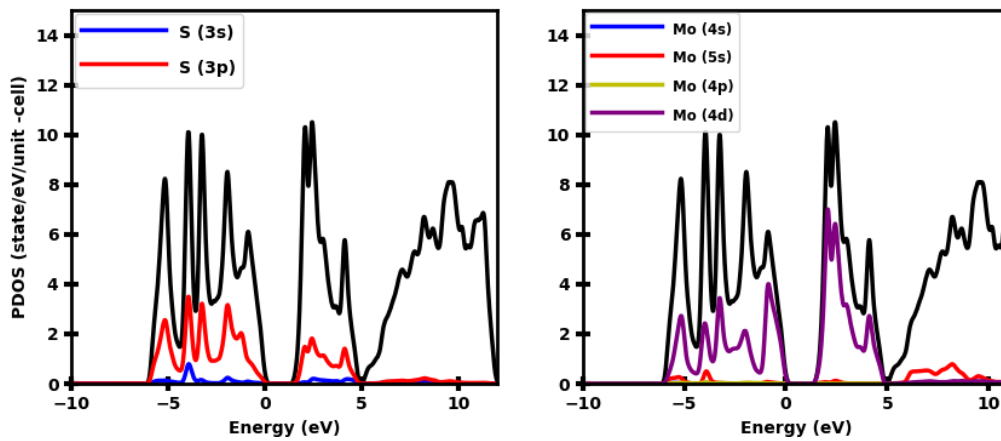


Figure 3.11: Above figure shows plot of TDOS and PDOS (Left) PDOS of sulfur (Right) PDOS of Molybdenum

As seen in Fig 3.11, the nature of the results are same as that in the case of monolayer. The reason for this was discussed in section 3.2 subsection 3.2.3.

3.4 Bulk

3.4.1 Convergence tests

Convergence tests similar to monolayer were performed for minimization of total energy of the system w.r.t to maximum allowed kinetic energy for wavefunctions (number of plane waves used), w.r.t to k point grid used for the Brillouin zone integration and sometimes also w.r.t to kinetic energy cutoff (Ry) for charge density and potential. The optimization helps us to reduce computational cost and get good accuracy in our results.

In the below figure convergence of total energy w.r.t to Ecut-wfc i.e. maximum allowed kinetic energy for wavefunctions was performed. The Kpoint mesh was set to 4 X 4 X 1 for this calculation.

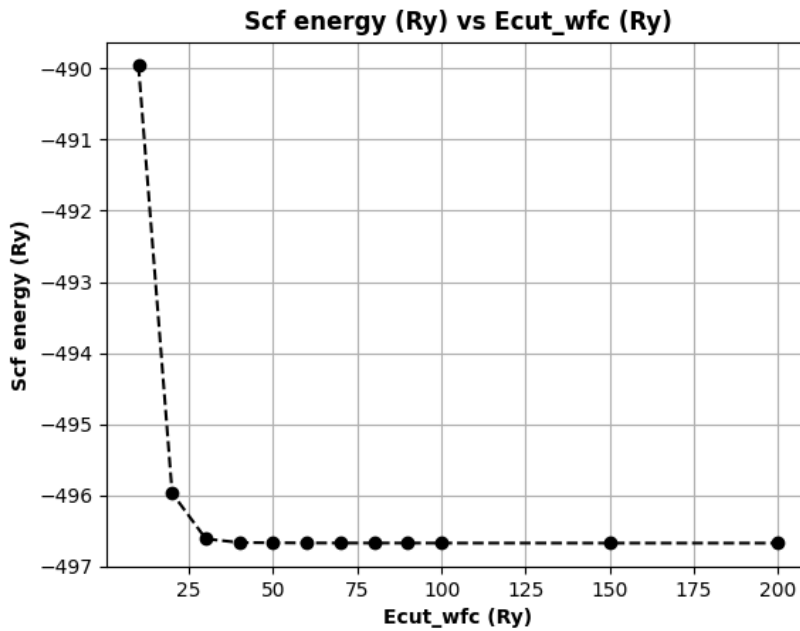


Figure 3.12: Above figure shows plot of SCF energy w.r.t kinetic energy cut off both in units of Ry.

In Fig 3.12 it can be seen that at a certain value of Kinetic energy cut off for wavefunctions the total energy of the system converges. Thus we can conclude from these that around 40-50 Ry value of Ecut-wfc is the optimum value to get good accuracy in the total energy of the system.

We also performed convergence of total energy w.r.t to K point mesh used for the Brillouin zone integration. For this calculation, the Ecut-wfc was set to 60 Ry. The k point values where varied from 16 to 196. In these fig, it can be seen that as the number

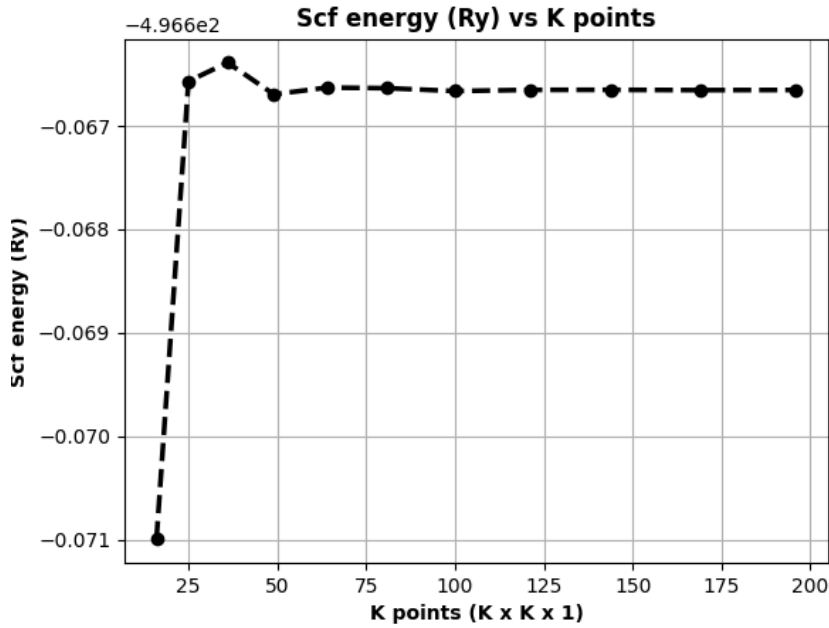


Figure 3.13: Above figure shows the plot of SCF energy w.r.t discretized k vector (or k points) grid.

of K points increases the variation in the total energy goes to almost zero. This indicates a proper convergence has been achieved. The optimum value of K points is 64 or 8 X 8 X 1. For subsequent calculations, this optimized value of Ecut-wfc and K points will be used (Unless explicitly mentioned).

3.4.2 Volume Optimization

The volume optimization was done to relax the bulk structure, and 7 exchange functions were used for volume optimization. By relaxing the bulk we obtained in-plane lattice constant, off off-plane lattice constant, and the interlayer distance between two layers. The

XC-functional	lattice constant - a	lattice constant - b	Interlayer spacing - d
GGA	3.1858	14.7244	7.3772
LDA	3.1241	11.9940	6.1277
vdw-df-c6	3.1681	12.2968	6.1952
vdw-df3-opt1	3.1585	12.2981	6.2147
vdw-df3-opt2	3.1642	12.3030	6.206
grimme-df2	3.1908	12.5283	6.2670
grimme-df3	3.1858	14.7244	7.3772

Table 3.4: The above table shows optimized in-plane constant-a and interlayer distance value using different types of XC functionals in \AA unit.

experimental values for the in-plane lattice constant remain the same as that in the case of monolayer i.e. 3.14 Å. The interlayer distance experimental value is around 6.15 Å. It can be seen from the table that vdw non-local functionals give a better estimate of interlayer distance with a percentage error of 0.02 %. GGA overestimates both lattice constant as well as interlayer spacing whereas LDA underestimates the same. The grimme-df2 and grimme-df3 which are DFT-D methods give almost the same results as those of GGA.

3.4.3 Electronic Properties

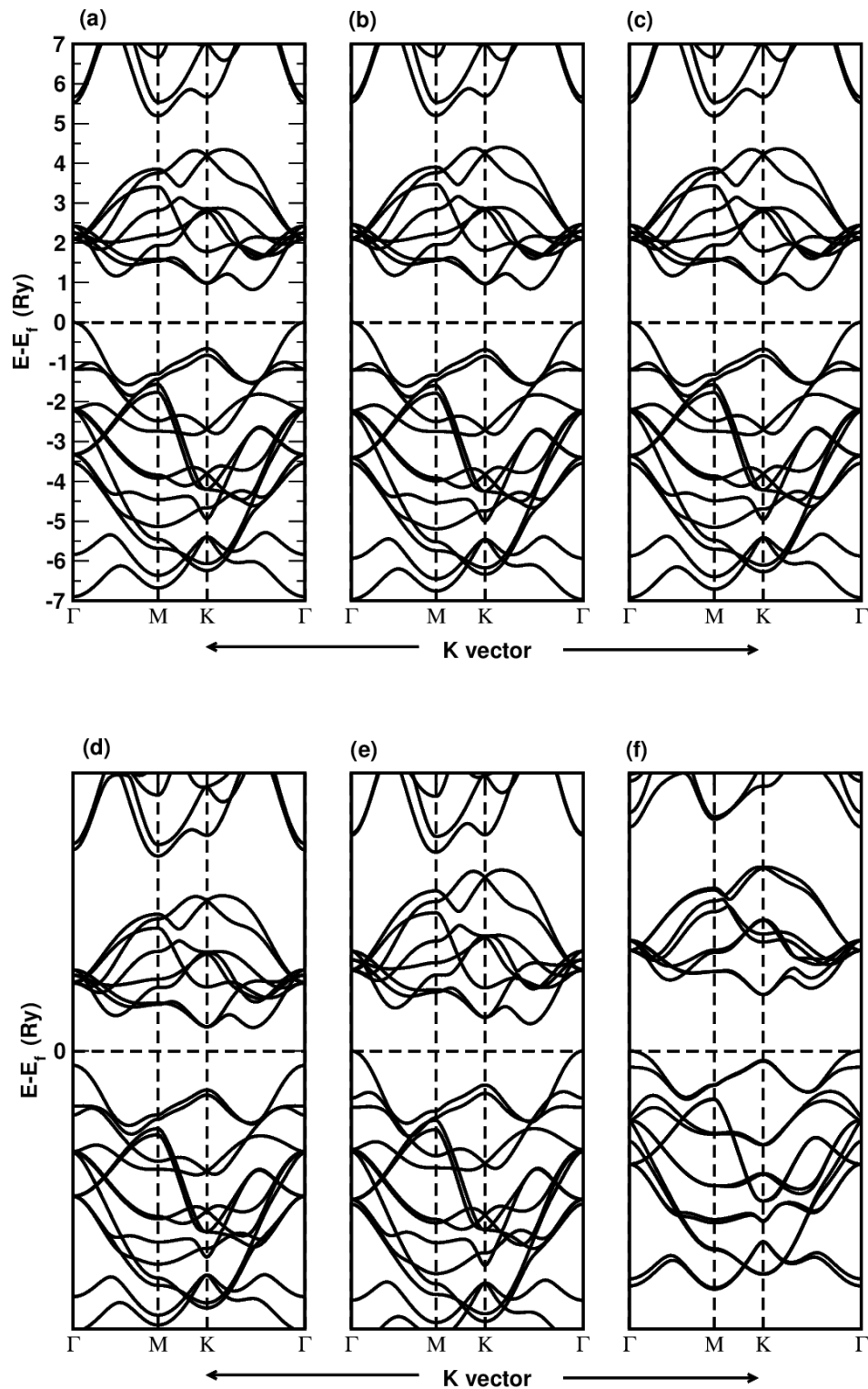


Figure 3.14: Above figure shows plot of electron dispersion curves of MoS_2 , a) Band structure obtained using vdw-df-C6 b) Band structure obtained using vdw-df3-opt1 c) Band structure obtained using vdw-df3-opt2 d) Band structure obtained using Grimme-df2 e) Band structure obtained using LDA f) Band structure obtained using GGA.

The above figure shows the band structure of MoS₂ bilayer. This band gap is obtained using PAW type pseudopotential and using 6 different XC-functional. It shows different band gap values depending on the type of XC-functional used for the calculation.

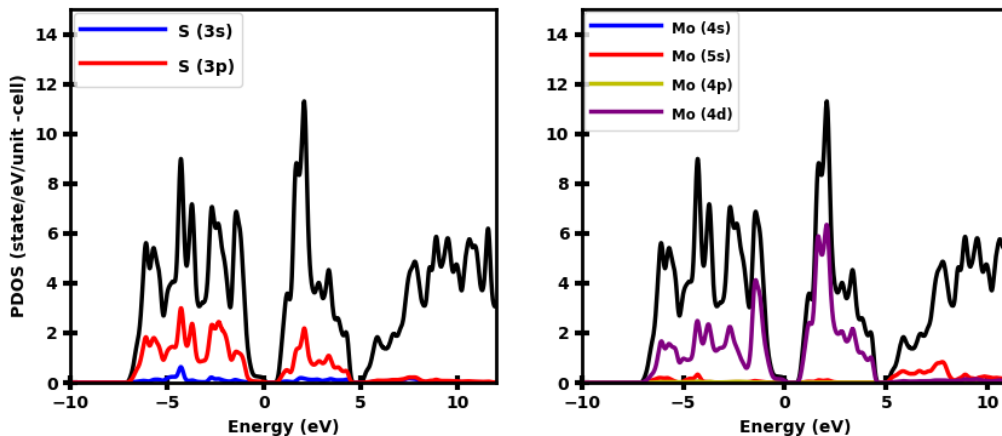
XC-functional	Experimental Band Gap	Band Gap obtained
vdw-df-C6	1.29 eV	0.826 eV
vdw-df3-opt1	1.29 eV	0.8368 eV
vdw-df3-opt2	1.29 eV	0.8229 eV
grimme-df2	1.29 eV	1.4479 eV
LDA	1.29 eV	0.68 eV
GGA	1.29 eV	1.32 eV

Table 3.5: Table showing Experimental value and Theoretical value of Bandgap for MoS₂ bulk for different XC-functional

Band structure of Bulk MoS₂ also shows indirect transition from Γ to between K- Γ high symmetry points. Again this nature is not observed in GGA and Grimme df methods. The reason for this is described in subsection 3.3.3 of section 3.3.

In the case of Bulk also the value produced by all XC-functional is not that accurate and has a huge deviation from the experimental value showing a 19-20 % relative percentage error. Also, plots of contributions of the individual atomic density of states or partial density of states to the total density of states were studied for sulfur atoms (S) and molybdenum atoms (Mo). The density of states calculation were done using the tetrahedron method. For this dense k-point grid was used i.e. 48 X 48 X 1 for proper sampling of the Brillouin zone.

Below are the plots for non-local functionals, Grimme df, LDA and GGA produced using PAW type pseudopotential.



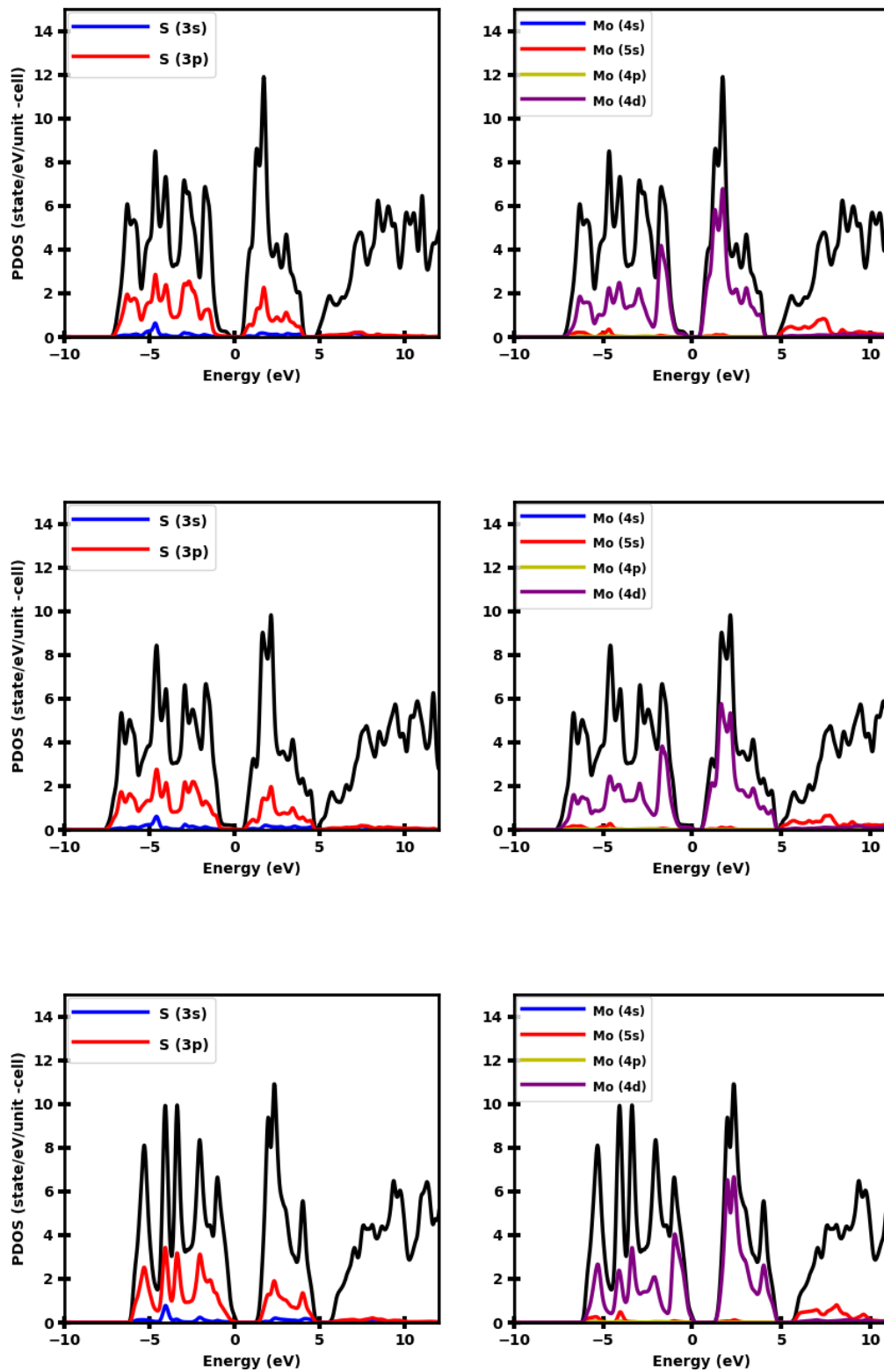


Figure 3.15: Above figure shows plot of TDOS and PDOS (Left) PDOS of sulfur (Right) PDOS of Molybdenum

As seen in Fig 3.15, the nature of the results are same as that in the case of monolayer. The reason for this was discussed in section 3.2 subsection 3.2.3.

We now compare the band structure of monolayer bilayer and bulk using functional which accurately shows the nature of band structure as shown experimentally in [1] [2].

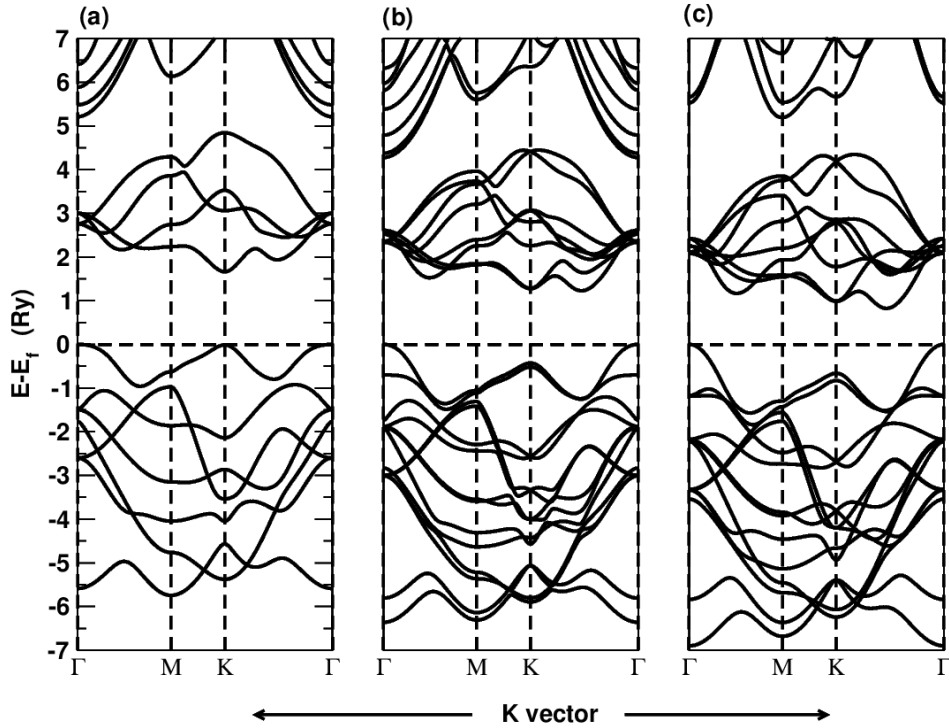


Figure 3.16: Comparison of the Band structure of a) monolayer, b) bilayer and c) bulk MoS_2

In the case of MoS_2 , the band gap undergoes a significant evolution as we move from a monolayer to a bilayer and finally to the bulk form. This evolution in band gap is due to quantum confinement effects and interlayer interactions [24]. In a monolayer of MoS_2 , the band gap is direct and has a larger value compared to that of bulk MoS_2 . As the number of layers increases, the band gap decreases and becomes indirect. This change in band gap is due to the increased interlayer coupling, which affects the electronic structure of the material [1].

Also, we compare the density of states of monolayer, bilayer, and bulk MoS_2 . The one key difference in the density of states plot of monolayer, bilayer, and bulk as seen in Fig 3.17 is the sharpness of the peaks. The monolayer density of states has sharp peaks which tend to get broader as we go from monolayer to bilayer and eventually to bulk. This is attributed to the phenomena of quantum confinement. The monolayer being an isolated layer with the weakest interlayer coupling among the three confines the electron motion in the layer itself. Hence the electronic wavefunction in the monolayer is highly localized compared to the other three thus giving rise to very sharp peaks. The bilayer and bulk

on the other hand have strong interlayer couplings which give rise to a more delocalized electronic wavefunction that increases the available energy states to occupy giving rise to the broader density of state peaks.

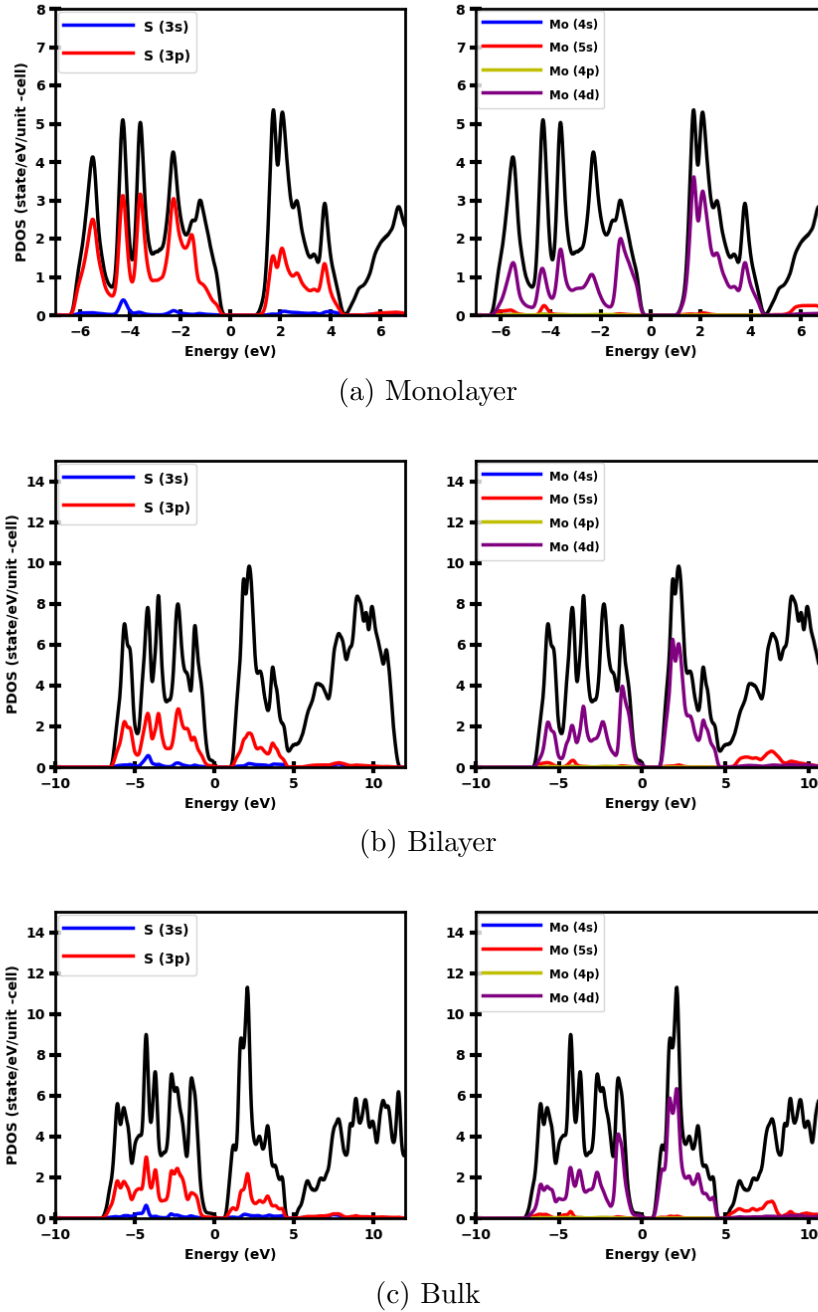


Figure 3.17: This figure compares of density of states of monolayer bilayer and bulk MoS_2

The planar charge density and planar potential energy plots were studied. These plots were used to understand better how interlayer spacing affects the nature of band gaps in MoS_2 bilayer and bulk. Below are the bilayer MoS_2 structure results. It can be seen from the both planar average charge and potential energy plots that GGA overestimates

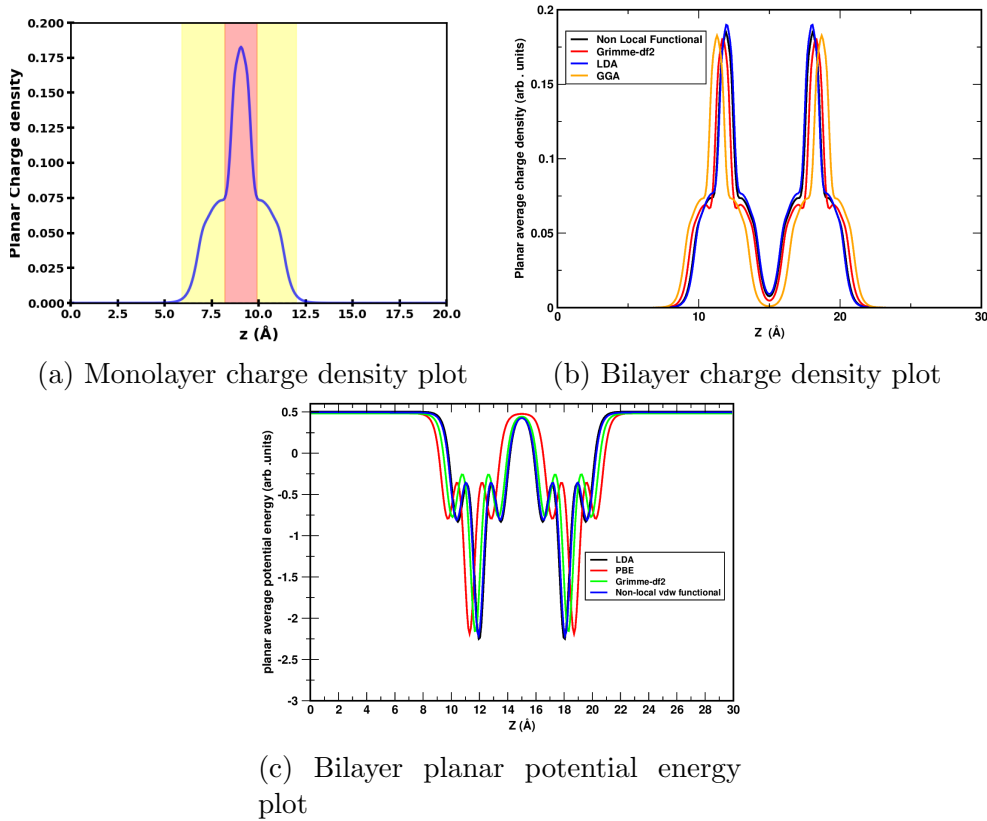


Figure 3.18: This figure compares the nature of planar charge density and planar potential energy for bilayer MoS_2 , subplot 3.18a is for reference and shows how Sulfur (yellow region) and Molybdenum (red region) contribute to planar charge density.

band structure. When vdw correction is added to GGA using grimme df2 [3] the planar charge density and planar average potential plot matches with that of non-local and LDA exchange-correlation functional.

References

1. Mak, K. F., Lee, C., Hone, J., Shan, J. & Heinz, T. F. Atomically Thin *nmathrmMoS_2*: A New Direct-Gap Semiconductor. *Physical Review Letters* **105**. [Online; accessed 2024-05-01] (Sept. 2010).
2. Conley, H. Bandgap Engineering of Strained Monolayer and Bilayer MoS₂. [Online; accessed 2024-05-01].
3. Grimme, S. Accurate description of van der Waals complexes by density functional theory including empirical corrections. *Journal of computational chemistry* **25**. [Online; accessed 2024-05-08], 1463–73 (Sept. 2004).
4. Hohenberg, P. & Kohn, W. Inhomogeneous Electron Gas. *Physical Review* **136**. [Online; accessed 2024-04-28] (Nov. 1964).
5. Carr, J. W. J., Coldwell-Horsfall, R. A. & Fein, A. E. Anharmonic Contribution to the Energy of a Dilute Electron Gas—Interpolation for the Correlation Energy. *Physical Review* **124**. [Online; accessed 2024-05-05] (Nov. 1961).
6. Gell-Mann, M. & Brueckner, K. A. Correlation Energy of an Electron Gas at High Density. *Physical Review* **106**. [Online; accessed 2024-05-05] (Apr. 1957).
7. Ceperley, D. M. & Alder, B. J. Ground State of the Electron Gas by a Stochastic Method. *Physical Review Letters* **45**. [Online; accessed 2024-05-09] (Aug. 1980).
8. Nusair, S. H. Vosko, L. Wilk, and M. Accurate spin-dependent electron liquid correlation energies for local spin density calculations: a critical analysis. [Online; accessed 2024-05-05] (Mar. 1980).
9. Perdew, J. P. & Zunger, A. Self-interaction correction to density-functional approximations for many-electron systems. *Physical Review B* **23**. [Online; accessed 2024-05-05] (May 1981).

10. Perdew, J. P. & Wang, Y. Accurate and simple analytic representation of the electron-gas correlation energy. *Physical Review B* **45**. [Online; accessed 2024-05-05] (June 1992).
11. Perdew, J. P., Burke, K. & Ernzerhof, M. Generalized Gradient Approximation Made Simple. *Physical Review Letters* **77**. [Online; accessed 2024-05-05] (Oct. 1996).
12. Giannozzi, P. *et al.* *Quantum ESPRESSO: a modular and open-source software project for quantum simulations of materials* <https://arxiv.org/abs/0906.2569>. [Online; accessed 2024-05-05]. June 2009.
13. Kohn, W. & Sham, L. J. Self-Consistent Equations Including Exchange and Correlation Effects. *Physical Review* **140**. [Online; accessed 2024-05-05] (Nov. 1965).
14. Wu, Q. & Yang, W. Empirical correction to density functional theory for van der Waals interactions. *The Journal of Chemical Physics* **116**. [Online; accessed 2024-05-09], 515–524 (Jan. 2002).
15. Grimme, S., Antony, J., Ehrlich, S. & Krieg, H. A consistent and accurate ab initio parametrization of density functional dispersion correction (DFT-D) for the 94 elements H-Pu. *The Journal of chemical physics* **132**. [Online; accessed 2024-05-08], 154104 (Apr. 2010).
16. Dion, M., Rydberg, H., Schröder, E., Langreth, D. C. & Lundqvist, B. I. Van der Waals Density Functional for General Geometries. *Physical Review Letters* **92**. [Online; accessed 2024-05-08] (June 2004).
17. Thonhauser, T. *et al.* Spin Signature of Nonlocal Correlation Binding in Metal-Organic Frameworks. *Physical Review Letters* **115**. [Online; accessed 2024-05-08] (Sept. 2015).
18. Lee, K., Murray, É. D., Kong, L., Lundqvist, B. I. & Langreth, D. C. Higher-accuracy van der Waals density functional. *Physical Review B* **82**. [Online; accessed 2024-05-08] (Aug. 2010).
19. Chakraborty, D., Berland, K. & Thonhauser, T. Next-Generation Nonlocal van der Waals Density Functional. *Journal of chemical theory and computation* **16**. [Online; accessed 2024-05-08], 5893–5911 (Sept. 2020).

20. Berland, K., Chakraborty, D. & Thonhauser, T. van der Waals density functional with corrected C_6 coefficients. *Physical Review B* **99**. [Online; accessed 2024-05-08] (May 2019).
21. Sabatini, R., Gorni, T. & de Gironcoli, S. Nonlocal van der Waals density functional made simple and efficient. *Physical Review B* **87**. [Online; accessed 2024-05-08] (Jan. 2013).
22. Coehoorn, R. *et al.* Electronic structure of $\text{nm}\mathit{MoSe}_2$, $\text{nm}\mathit{MoS}_2$, and $\text{nm}\mathit{WSe}_2$. I. Band-structure calculations and photoelectron spectroscopy. *Physical Review B* **35**. [Online; accessed 2024-05-01] (Apr. 1987).
23. Sun, L. *et al.* Spin-Orbit Splitting in Single-Layer MoS_2 Revealed by Triply Resonant Raman Scattering. *Physical Review Letters* **111**. [Online; accessed 2024-05-01] (Sept. 2013).
24. Das, S. Synthesis, Properties, and Applications of 2-D Materials: A Comprehensive Review. *Critical Reviews in Solid State and Materials Sciences*. [Online; accessed 2024-05-01] (July 2014).